

Evolutionary bursts drive morphological novelty

5

Ian G. Brennan ^{*1,2}, David G. Chapple³,
J. Scott Keogh², Stephen Donnellan^{4,5}

¹Natural History Museum, Cromwell Road, London SW7 5BD, UK

²Division of Ecology & Evolution, Research School of Biology,
Australian National University, Canberra, ACT 2600 Australia

³School of Biological Sciences, Monash University
Clayton, VIC Australia

⁴ School of Biological Sciences, The University of Adelaide,
Adelaide, SA Australia

⁵South Australian Museum, North Terrace, Adelaide SA 5000 Australia

10 *Keywords:* Morphological evolution, Simpsonian, skink phylogenomics.

*Corresponding author: iangbrennan@gmail.com

Summary

Animals come in all shapes and sizes. From mundane to bizarre, their features are the result of millions of years of evolution and mutation accumulating differences and adjusting designs. As a result of differing selective pressures and drift phenotypes evolve and diverge.

15 However there is little consensus about the evolutionary mode of most traits and if novel morphologies evolve from prolonged (Darwinian gradualist) or episodic (Simpsonian jump) divergences. Here we use novel exon-capture and linear morphological datasets to investigate the tempo and mode of morphological evolution in Australo-Melanesian Tiliquini skinks. We generate a well-supported time-calibrated phylogenomic tree from 400 single-copy nuclear
20 markers for 77 specimens including undescribed diversity, and provide unprecedented resolution of the rapid Miocene diversification of these lizards. By collecting a morphological dataset that encompasses the lizard body plan (21 traits across the head, body, limb, and tail) we are able to identify that most traits evolve conservatively but infrequent evolutionary bursts result in morphological novelty. These phenotypic discontinuities occur via rapid
25 rate increases along individual branches, inconsistent with both gradualistic and punctuated equilibrial evolutionary modes. Instead, this ‘punctuated gradualism’ has resulted in the rapid evolution of blue-tongued giants and armored dwarves in the ~20 million years since colonizing Australia. These results outline the evolutionary pathway towards new morphologies and highlight the heterogeneity of evolutionary tempo and mode, reconciling Darwinian
30 and Simpsonian evolution.

Introduction

Great variations in organismal morphology are expected to accumulate over long periods of time and reflect the varied requirements of different species^{1,2}. Some organisms are very small and some are very large, others are brightly colored and others cryptic, and through drift and selection, traits respond and diverge from common forms. But despite the dramatic variation we see in nature, when we look closely, measures of these differences (variance, disparity, *et al.*) almost always fail to exceed the expectation of a neutral model where the accumulation of variation is the result of a random evolutionary walk through time (Brownian Motion)^{3,4}. In other words, Earth's flora and fauna realize only a fraction of all possible shapes and sizes⁵. This diversity undershoot suggests bounds on phenotypes as a result of genetic, functional, or developmental constraints^{6,7}. If this is the case, then how do novel morphologies arise? And what does the mode of morphological evolution look like if not gradual?

When traits are assumed to evolve under an unbiased random walk (Brownian Motion), trait variance (v) is proportional to evolutionary rate (σ^2), and the accumulation of variance is dictated by elapsed time (t ; so $v=\sigma^2 t$). This exploration of trait space (diffusion) is characterized by trait change along branches drawn from a normal (Gaussian) distribution, and assumes a flat adaptive landscape^{8,9}. Given observed trait limits, correlations among traits, and the “clumpiness” of extant morphological diversity, this seems an unlikely expectation^{2,10}. In practice, morphological evolution is often concentrated on one or a small number of major axes. The primary axis serves as a ‘line of least resistance’¹¹ providing a pool of variation on which selection can act. However evolution is not limited to the major axis, and trajectories along minor axes may also pave a path towards new phenotypes. These competing processes have been termed “elaboration” (*along* major axis) and “innovation” (*away* from major axis)^{12,13}. However their relative contributions towards organismal macroevolution and the evolution of novel forms has been largely overlooked¹³.

Almost 80 years ago G.G. Simpson suggested novelty arose by rapid “jumps” to new adaptive zones across an uneven landscape¹⁴. To explore this landscape, one potential path requires relaxing our assumption that traits evolve consistently across lineages—changing the *mode* of evolution. Proposed alternative evolutionary models such as pulsed or punctuated processes account for rapid jumps in just such a way—by deviating only in the evolutionary *mode*—leaving variance to accumulate as under BM. Another pathway however requires relaxing our assumption that traits evolve via constant rates through time—changing the *tempo* of evolution. These relaxed-rate methods are implemented in Variable Rates or Multi-Regime models of trait evolution. Traditionally, jumps have been difficult to identify without fossil data. This is due in part to the limited information content at internal nodes of a phylogenetic tree, however, even in fossil studies debate has continued about gradual versus pulsed/punctuated evolution^{15,16}. Recent advances in phylogenetic comparative methods however, provide the tools to distinguish between gradual and punctuated evolutionary modes, and suggest that pulsed evolution and rate heterogeneity may be common processes^{17–22}.

When studying the morphological evolution of any empirical group differences in evolutionary mode and tempo are potentially compounded by mosaic evolution—which suggests that processes may vary widely across individual traits and the modules they make up. So when looking for macroevolutionary shifts towards new phenotypes, changes may be tempo-

75 rally, phylogenetically, or regionally (across the body) heterogenous. Just a century ago these complications seemed impossible to address: “To select a few of the great number of structural differences for measurement would be almost certainly misleading; to average them all would entail many thousands of measurements for each species or genus compared”²³. Modern comparative methods however, have made these comparisons possible. Here we
80 investigate the relative roles these sources of variation play, by focusing on the Tiliquini skinks. Tiliquines consist of ~62 species with varied ecologies, high levels of sociality^{24,25}, and highly imbalanced biogeographic richness. The majority of species (~48 spp.) are endemic to Australia where their distributions span the continent’s highest alpine peaks and most inhospitable deserts. To survive in such varied climes, tiliquines have diverged into
85 herbivorous giants that roam the treetops, spiky socialites that live communally in rock crevices or complex burrows, and elongate long-lived slow-movers that wander across open lands. These ecotypes have diagnosable morphologies, and the modest species richness of the group allows high-dimensional macroevolutionary study to be computationally tractable. Additionally, tiliquines are ideally suited for studies of the tempo and pace of morphological
90 evolution because they have been suggested to represent a plesiomorphic grade with highly derived morphotypes nested deeply within the phylogeny^{25,26}.

But to what degree are these morphological deviations *remarkable*, and what tempo and mode have they evolved by? To answer these questions we started by generating an exon-capture dataset for Tiliquini skinks and reconstructing the phylogenetic relationships of this
95 group. To look at morphological evolution we collected an extensive phenotypic dataset of 21 linear measurements which summarize broad axes of variation across the head, body, limbs, and tail. Finally we incorporate these data into a multivariate framework for comparing evolutionary rates and disparity of traits (and the modules they compose) relative to a neutral BM model of evolution. From this we are able to show that (1) most traits show
100 heterogeneous—not neutral or incremental—evolutionary histories, (2) evolutionary bursts are temporally and phylogenetically distributed but uncommon, and (3) these jumps result in morphological novelty that can exceed uncorrelated trait expectations.

Results

Phylogenetic Analyses and Divergence Dating

105 We present a well-resolved phylogeny that provides unprecedented resolution of Tiliquini skinks representing all genera and 53 taxa (77 samples) across this continental lizard radiation. Concatenated (Fig.S7) and coalescent-consistent species trees (Fig.1) return broadly similar topologies with the exception of a handful of extremely short internal branches (Fig.S8). Discordant branches fall within the anomaly zone²⁷ in which concatenation is
110 likely to be mislead by the contribution of a large number of anomalous gene trees. In support of this, these nodes as represented in our coalescent species tree generally have low gene concordance factors (gCFs) and equivocal site concordance factors (sCFs), but are strongly supported by individual topology tests (see Supplementary Materials **Topology Tests**). Of these contentious nodes, two have taxonomic implications. *Lissolepis* is not recovered as
115 monophyletic, with *L. coventryi* estimated as sister to *Liopholis*, and *L. luctuosa* more closely

related to the remaining tiliquines (*Cyclodomorphus*, *Tiliqua*, *Bellatorias*, *Egernia*). We also find *Cyclodomorphus* to be non-monophyletic, with the *C. gerrardii* group more closely allied with *Tiliqua* than with the *C. maximus* group.

Branches that define many of the inter-generic relationships among Australian tiliquines

120 are the result of a series of rapid speciation events occurring 15–21 mya. Most of these branches are shorter than a million years long, and several of which are less than 500k years long. These rapid divergences contrast with the deep splits between Australian tiliquines and their sister taxon *Corucia* (30 mya; 95% HPD: 27–35 mya), as well as the preceding split from *Tribolonotus* (60 mya; 95% HPD: 55–64 mya) (Fig.1,S1).

125 Phenotypic Analyses

Modularity and integration model selection in *EMMLi*²⁸ identified a four module model with separate within module correlations (intramodule integration varies among modules) and separate among module correlations (intermodule integration varies among modules) as the best fit to our data.

130 13 of 19 morphological traits are best fit by variable rate or pulsed models (Fig.S6). The abundant preference for heterogeneous evolutionary models encouraged us to focus on the evolution of traits and modules under the Variable Rates model for all further analyses. The major axis of morphological variation (elaboration; PC1) across the Tiliquini and across each genus is primarily explained by tail length (Fig.S20—S22). The major axis of morphological innovation (PC2) varies when considering the clade as a whole (interlimb length) or individual genera (primarily size and/or interlimb length). The relationship between elaboration and innovation, however, varies among genera. We visualize this through varied slopes between our first two PC axes, highlighting different paths to phenotypic novelty (Fig.2).

135 With few exceptions, trait variance accumulated more slowly through the first 40 million years of tiliquine evolution than under the BM null model, for both individual traits (Fig.S16) and modules (Fig.3). Comparing the slopes of these accumulation curves highlights periods of significant morphological conservatism (tail module 20–15 mya) and expansion (body and limb modules 18–14 mya; tail module 3 mya–present). Periods of expansion generally—but not always—coincide with periods of increased mean evolutionary rates (Fig.3). Discretizing 140 morphological change as primarily elaborative or innovative allows us to identify that both processes happen at clade and species-level scales (Fig.2).

Averaging rates however, hides pulses of extreme rate variation (Fig.4). We identified 145 pulses by isolating branches with at least twice the background evolutionary rate (mean scalar $r \geq 2$) that were shifted in at least 70% of the sampling posterior. Across 19 focal traits, roughly 13% branches exhibited a significant rate pulse, with more than 3% showing major shifts in evolutionary rate (mean scalar $r > 10$) (Fig.S14). Major shifts were primarily concentrated in head width, interlimb length, tail length and width, and upper arm length. In modules, nearly 16% of branches exhibited significant rate pulses, with 2% showing major shifts, concentrated in tail and body modules. Many rate increases are concentrated in 150 the *Cyclodomorphus*–*Tiliqua* clade, with particularly rapid rates among *Cyclodomorphus michaeli*, *casuarinae*, and *praealtus*. Body and tail traits also commonly show rate pulses in the crevice dwelling *Egernia stokesii* and *depressa* clades. Under relaxed-rate models rate pulses transfer into bursts in morphological change. We are able to visualize these 155

morphological jumps along individual branches (Fig.6), highlighting moments which lead to
160 novel phenotypes.

Simulations under uncorrelated and correlated Brownian Motion show differences in the accumulation of trait combinations. This highlights how evolution can be biased along particular axes (Fig.5, S5). Empirical traits generally conform to BM expectations, however extreme phenotypes exceeding BM predictions have evolved in the feet of *Tiliqua* and tails
165 of some *Egernia* (Fig.5, S9–S13).

Discussion

The variety of organismal forms has been a bottomless well of inspiration for scientists and the public, and an almost infinite source of data for macroevolutionary biologists to investigate the timing and accumulation of morphological diversity. Whether morphological disparity has accumulated early¹, uniformly²⁹, or via intermittent pulses^{2,18,21} remains a contested topic at varied evolutionary scales. Here we investigate the morphological evolution of the lizard body by looking across time, phylogeny, and body regions to better understand the modes by which traits evolve. We provide evidence for Tiliquini skinks that most traits evolve conservatively, but morphological novelty accumulates through extreme punctuations—jumps into new trait space. These jumps are uncommon (0.003–0.05 jumps/my), do not follow an established morphological order³⁰, and can be nested to develop new trait combinations.
170
175

Phylogenomics of the Tiliquini

Skinks are a tremendously species rich group that make up more than 25% of all lizard diversity (1700+ species). The largest and most impressive skinks belong to the tribe Tiliquini which are primarily distributed across Australia with a small number of species found in Indonesia, Papua New Guinea, and the Solomon Islands. Despite their importance as models of reptilian sociality^{24,31} and as an emerging fossil system^{26,32,33} phylogenetic hypotheses for the Tiliquini have relied on a handful of molecular markers and limited species sampling^{25,34,35}.
180
185 Our exon capture dataset provides a well supported estimate of the relationships among all eight Tiliquini genera and 80% of described species. In agreement with previous estimates we recover the Tiliquini as members of the Lygosominae alongside the Sphenomorphini, Eugongylini, and Mabuyini (Fig.S1), suggesting an Asian origin for the subfamily³⁶.

Living tiliquines are divided into three clades, comprising the enigmatic Crocodile Skinks
190 *Tribolonotus*, the monotypic Solomon Islands endemic *Corucia*, and an Australian radiation. Splits among these groups are old (~60 & ~30 mya), and followed by the rapid Miocene divergence of all Australian Tiliquini genera (23–15 mya). These rapid speciation events result in short internal branches that prove difficult to resolve on a per-locus basis (Fig.1,S18). However, most of these difficult nodes are resolved by leveraging our 400 loci in ASTRAL,
195 investigating summary statistics, and applying topology tests. Our new phylogenetic hypotheses of these nodes has necessitated that we propose taxonomic changes for two genera, which we provide in the attached Appendix ([Taxonomic Implications and Changes](#)). Some splits remain intractable however. The branching patterns among major *Egernia* clades,

and the series of splits among *Lissolepis luctuosa*, *Liopholis*, and the remaining Australian tiliquines have splits so short (300–400ky) that they exist at the limits of phylogenetic reconstruction. Regardless of resolution of these difficult branches, the radiation of Australian Tiliquini into divergent ecologies and morphologies happened rapidly and in concert across open landscapes, closed forests, deserts, and mountain peaks.

Evolving Novel Phenotypes by Bursts

Earth's incredible biodiversity of forms and functions have evolved over hundreds of millions of years. Growing evidence suggests that much of this diversity accumulated via short periods of rapid phenotypic change, not by incremental divergence^{18,21,37,38}. If this is true and pulsed morphological evolution is common, then it is important to understand how it contributes to the development of morphological novelty and diversity. To do this we identified how pulses are distributed through time, across the phylogeny, and among morphological axes.

Much of modern macroevolutionary thinking relies on Simpson's (1944) idea of adaptive zones. The varied adaptive landscape accumulates diversity as lineages traverse into new adaptive zones that are centered around fitness peaks. Lineages move into new zones by evolutionary jumps—rapid movement across suboptimal space. In comparative studies the idea of a multipeak morphological landscape is often described by multi-optima OU models^{39–41}. While these models account for the clustering of species around discrete trait values (evolutionary ‘clumpiness’) they do not explain well the process of movement across the landscape to occupy new peaks. Our analysis of the lizard body plan provides evidence that pulses in evolutionary rate and coincident phenotypic change are common across many morphological traits (preferred in 13 of 19 traits). This suggests that large distances of suboptimal trait space can be quickly traversed to reach new morphological realms. When comparing modeled empirical data to gradualist simulations, jumps are observable as large trait changes along individual branches (Fig.6). However, the accumulation of morphological disparity does not appear to be dictated solely by rare jumps, or to occur explicitly at speciation, as in the punctuated equilibrium model of⁴². Instead, we find broad support for a model in which the background process of evolution by a random walk (Brownian Motion) is punctuated by bursts in evolution that result in jumps to new adaptive zones. We consider this process more akin to the “punctuated gradualism” model of Malmgren et al. (1983). While we recognize that our inferred process is not entirely consistent with⁴³ who proposed punctuations between evolutionary stasis and gradualism, we suggest that these distinctions may instead be indicative of similar processes occurring at different scales along the micro-to-macroevolutionary continuum. At both scales, a heterogeneous mode driven by an increase in evolutionary rates facilitates the evolution of novel and divergent morphologies (Fig.4)—in the case of these lizards, this occurs against a background morphological diffusion process. In this way we attempt to find common ground for both Darwinian and Simpsonian evolution.

In the Variable Rates model branch-specific shifts are indicative of an increase in evolutionary rate but remain a parameter of a random walk (Brownian) process. So, increasing the evolutionary rate suggests an increase in the *evolvability* and ultimately the potential variance of a lineage. An alternative interpretation of our identification of rate bursts could instead be a directional (biased) trend towards distinct trait values. A recently designed

method for addressing this—the *fabric* model of *BayesTraits*⁴⁴—proposes that excess rate estimates could instead be absorbed by a biased walk to new trait space. Importantly, this does not fundamentally change the outcome that evolution has swerved into a new morphological lane, but it does suggest a difference in the evolutionary mode. Whereas a rate pulse suggests a rapid, random exploration of trait space that lands in a new zone, directional trends elicit a guided evolutionary walk (e.g. via selection) towards a new area of trait space. Because a guided walk is directional the evolutionary rate need not be rapid. Regardless, the jump in trait value along a branch, and evolution of a new phenotype remains the same.

This provides an appealing explanation for scenarios where selection might be particularly effective, such as in small populations or those with high trait variances.

Importantly, inferred phenotypic jumps happen along both the primary morphological axis—where they exaggerate existing variance (elaboration)—and along minor morphological axes—where they develop novel trait combinations (innovation). Along both major and minor axes relatively uncommon but major discontinuities result in unusual and novel morphologies, as seen in birds⁴⁵ and fish⁴⁶. In Tiliquini skinks, the most obviously novel phenotypes belong to the Bluetongue lizards *Cyclodomorphus* and *Tiliqua*. Bluetongues concurrently underwent dramatic shifts in limb and body modules, extending the length of the body and shortening the limbs. Subsequent jumps in head and tail modules resulted in further temporally staggered morphological bursts. These nested morphological pulses gave rise to broad heads and bodies, dwarfed extremities and stumpy tails in *Tiliqua*, highlighting that truly new morphologies can arise from rapid exploration of multiple body axes. However, some of the most dramatic changes have happened on the shortest timescales. In the *Cyclodomorphus michaeli* clade (*C.casuarinae*, *C.michaeli*, *C.praealtus*) which we estimate at less than 4 million years old, we identify jumps in tail, limb, and body traits. These result in the rapid shortening of the interlimb, tail, and leg lengths in *C.praealtus*, and lengthening of these traits in *C.casuarinae* and *C.michaeli*. Interestingly, these changes are potentially driven not by functional morphological reasons but instead by physiological ones. *C.praealtus* lives at high elevations where shortened extremities may be advantageous to maintain thermal mass following Allen’s Rule⁴⁷.

Occasionally independent evolutionary trajectories arrive at similar adaptive zones, a process usually called morphological convergence. We identify convergence in the spiny crevice-dwelling clades of *Egernia* (*E. stokesii* and *E. depressa*). These clades have undergone rapid shortening and widening of the tail from non-armored, long-tailed ancestors (Fig.4). Amazingly, these clades have both arrived at this novel phenotype via rate increases of roughly ten times the background rate. The repeated evolution of a distinct phenotype like highly modified tails suggests strong selective pressures shaping some morphological axes⁴⁸. Another example of the strength of selection concerns the only clade of primarily crepuscular and nocturnal tiliquines the *Liopholis kintorei-inornata* group. This clade is broadly distributed across arid and semi-arid Australia, living in burrows they dig in loose soil or sand. However, the transition of these skinks towards a nocturnal lifestyle does not appear to have driven exceptional morphological differentiation from other *Liopholis*, except for the size of their eyes. The transition in diel activity is coincident with a jump in eye diameter and even the evolution of vertical pupils in the Night skink *Liopholis striata* (Fig.S14). Despite the evolution of novel morphologies by phenotypic bursts, truly exceptional morphologies (those exceeding Brownian expectations) are rare. In a few cases, such as the feet of some

Tiliqua and the tails of some *Egernia*, contemporary trait values fall outside what we expect under a uncorrelated random walk model. These instances provide the strongest cases for active selection driving the evolution of phenotypes (Fig.5).

290 **Conclusions**

Animal bodies are made up of many morphological traits which in their myriad combinations contribute to Earth's amazing biodiversity. This diversity has diverged from common forms on deep temporal scales, however our understanding of this process has begun to question the popularity of commonly invoked Darwinian gradualism as its driver. Our study of gross lizard 295 morphology provides evidence instead that trait evolution is heterogeneous, and is structured phylogenetically, temporally, and across the body-plan. This adds to a growing body of evidence that morphological traits diverge through evolutionarily discontinuous processes. These discontinuities contribute substantially towards the evolution of novel morphologies, and we suggest that this is likely a common process in morphological diversification across 300 animals that helps reconcile Darwinian and Simpsonian evolution.

Acknowledgments

A considerable thank you to the curators and staff of the many Australian museums and databases for access to tissues and locality data that made this work possible. We greatly appreciate the assistance of Emily Lemmon Moriarty, Alan Lemmon, and Michelle Kortyna 305 in generating AHE data for this project. We thank Mark Hutchinson and Kailah Thorn for sharing their expertise in Tiliquini skinks, and colleagues in the Natalie Cooper lab at the NHM for their insight. JSK, SCD, and DGC thank the Australian Research Council for ongoing support, including grant LP170100012 to DGC. IGB is supported by a Marie Skłodowska-Curie Fellowship funded by the European Commission.

310 **Author Contributions**

Conceptualization, IGB, JSK, SD; sampling, JSK, SD.; analysis, IGB; funding acquisition/resources, JSK, SD, DCG; data curation, DCG, IGB; writing—original draft, IGB; writing—reviewing & editing, all authors.

Competing Interests

315 The authors recognize no conflicts of interest, either direct or indirect, that might bias the conclusions, implications, or opinions stated in this work.

Figures

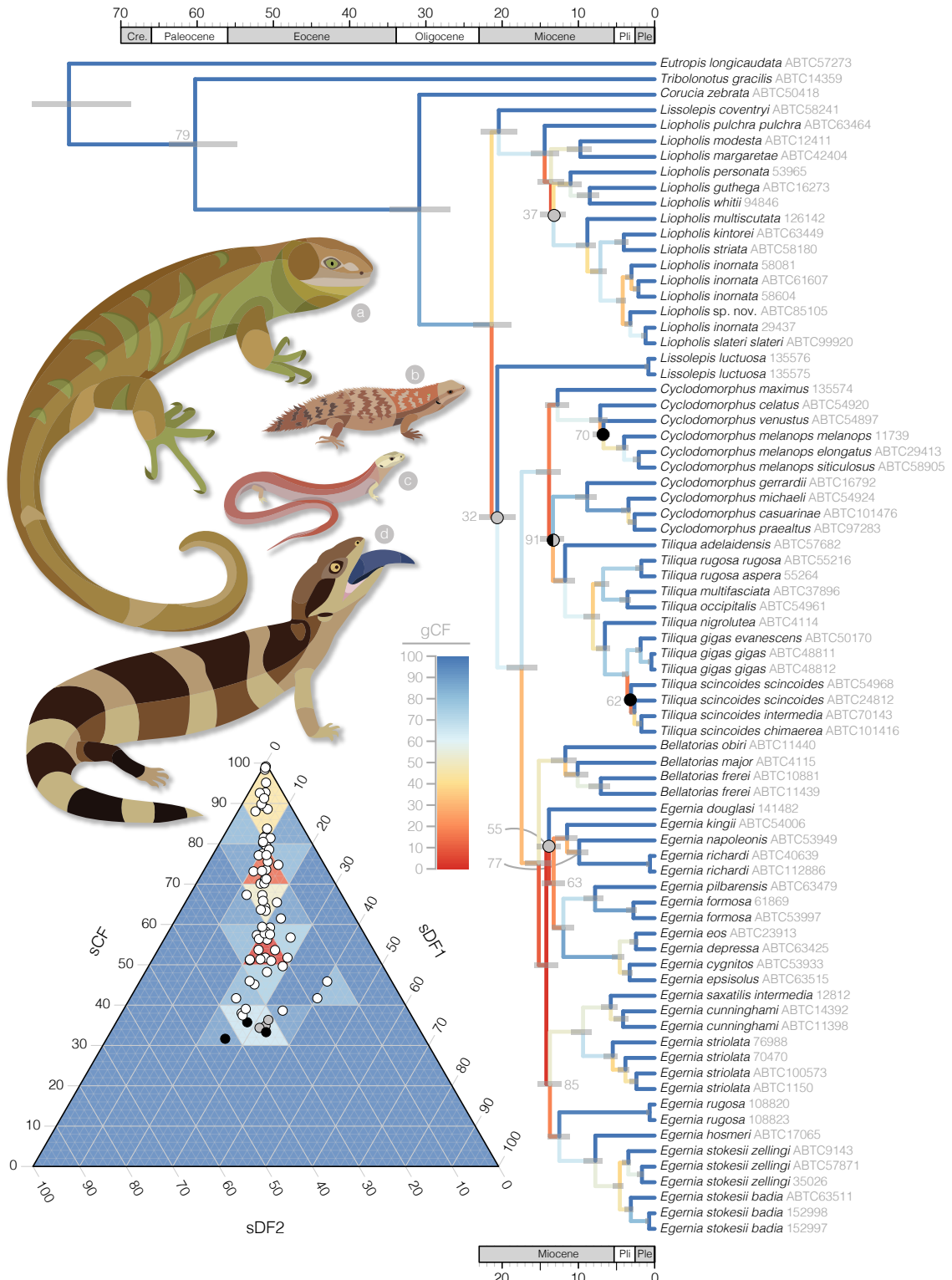


Figure 1: Species tree caption below.

Figure 1. The species tree estimated with ASTRAL and time-calibrated with MCMCTree shows late Oligocene or early Miocene divergences of most major Australian Tiliquini skinks, in contrast to a Paleocene divergence from *Tribolonotus* and early Oligocene divergence from the monotypic *Corucia*. Local posterior supports for all nodes are 100, except where indicated by grey numbers. Branches are colored according to gene concordance factors (gCF)—the proportion of gene trees which decisively support the given bifurcation—as estimated by IQ-TREE. The ternary plot bottom left shows the distribution of site concordance factors (sCF) for all nodes in the presented tree. sCFs provide another way of interpreting uncertainty by showing relative support for alternative resolutions of a given bifurcation (sDF1, sDF2). sCF values plotted in black on the ternary plot and corresponding tree highlight nodes where $sCF < sDF1$ or $sCF < sDF2$, meaning the bifurcation presented on the tree is not supported by the majority of sites in the concatenated alignment. sCF values plotted in grey on the ternary plot and corresponding tree highlight nodes where $sCF \approx sDF1 \approx sDF2$, suggesting an unresolved polytomy. Animals illustrated are (a) *Corucia zebrata*, (b) *Egernia depressa*, (c) *Cyclodomorphus michaeli*, and (d) *Tiliqua scincoides*.

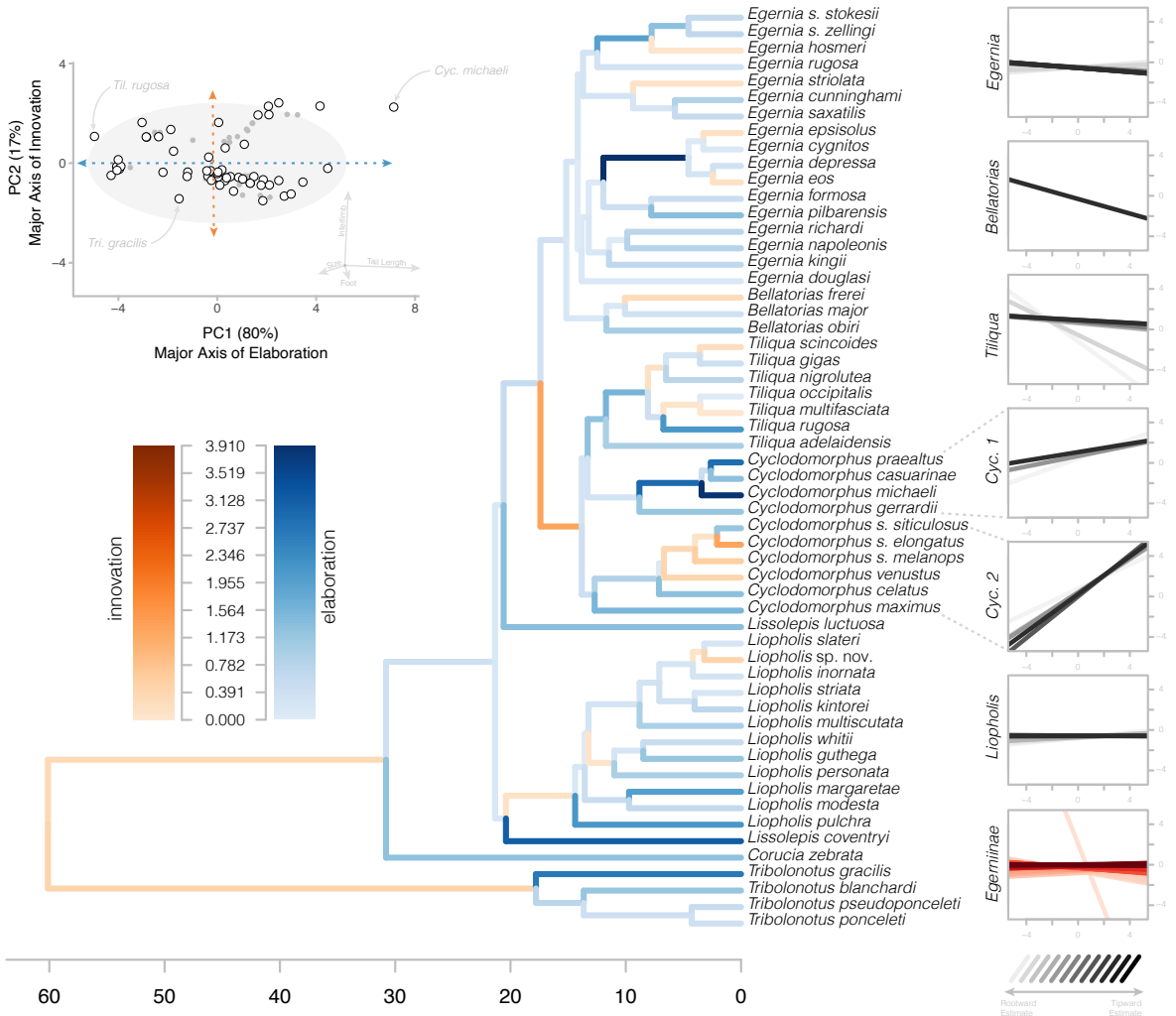


Figure 2: Major and minor axes of morphological change allow us to identify moments of elaboration (along PC1-blues) and innovation (along PC2-oranges) in Tiliquini skinks. Top left—biplot of first two principal components show the distribution of observed species (white circles with black outlines) and estimated ancestors (grey circles) along the major axis of elaboration and innovation. Colored branches on the tree at center indicate the primary direction of morphological change from ancestor to descendant node. Blue branches indicate principally elaborative change, while orange branches indicate principally innovative change. At right we visualize the varied relationships between these axes among groups. For each clade (genera and group as a whole) we plot the evolution of the relationship between elaborative and innovative axes through time from the root of the clade (lightest regression) to the tips (darkest regression). Regression plots highlight the varied patterns of subclades, including strong conservatism of *Liopholis* and novelty of *Cyclodomorphus*.

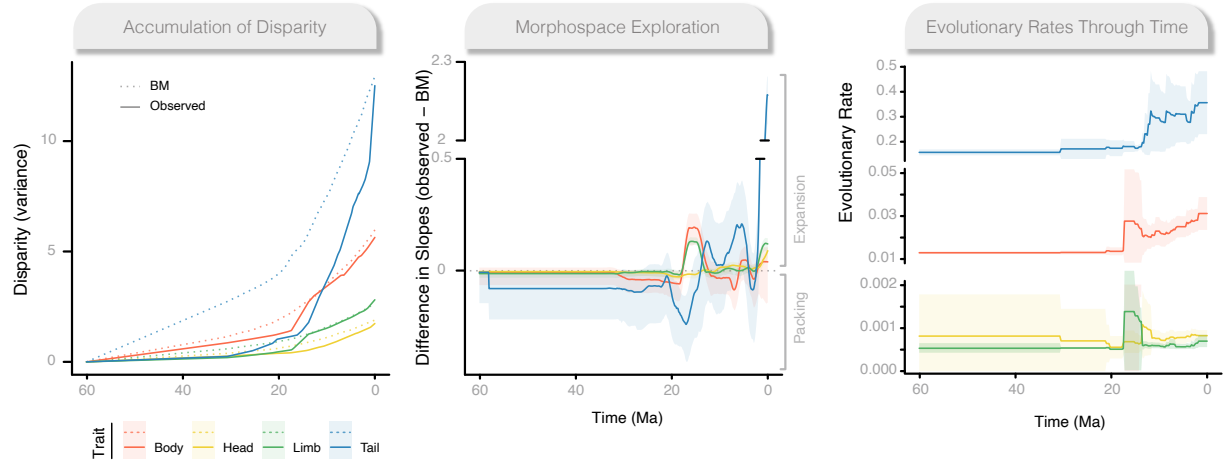


Figure 3: Evolutionary trajectories vary widely across modules and through time. (left) Accumulation of multivariate disparity (as variance) through time for each module (solid lines) compared to Brownian Motion (dotted lines). (center) The comparison of slopes of each module to BM highlights periods of morphological expansion (values greater than 0) and conservatism (values less than 0). (right) Evolutionary rates across modules are highly heterogeneous (see three different scales for y axis), showing periods of temporal variability, as well as high variances within modules and among traits (Fig.S15–S17).

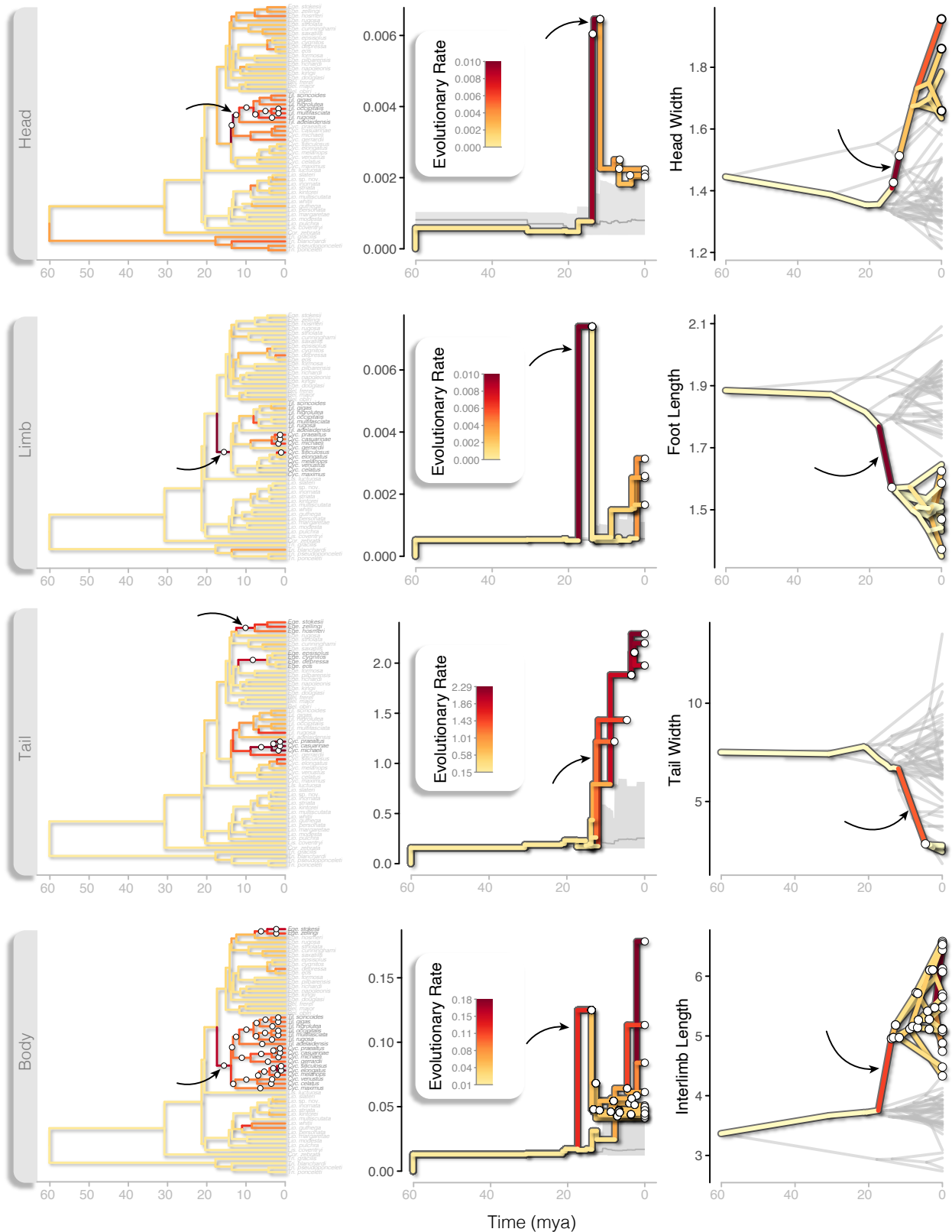


Figure 4: Rates caption below.

Figure 4. Bursts in rates of phenotypic evolution are distributed across the Tiliquini tree and exhibit strong departures from background rates. Rows represent morphological modules. In all plots branch colors correspond to estimated multivariate evolutionary rates, with significant rate changes noted by white circles at nodes or along branches. (left column) Tiliquini species trees highlighting the location of multivariate rate pulses. (center column) Branch rate trajectories plotted from the root node to nodes that show significant rate shifts (estimated rate scalar $r > 2$). Solid grey envelope contains 95% quantiles of background evolutionary rates (estimated rate scalar $r < 2$) with the mean plotted in dark grey. (right column) Phenograms of an individual trait from each module showing the evolution of extreme phenotypes driven by bursts in evolutionary rate. In each row, a black arrow highlights a single branch of interest across all three plots.

335
340

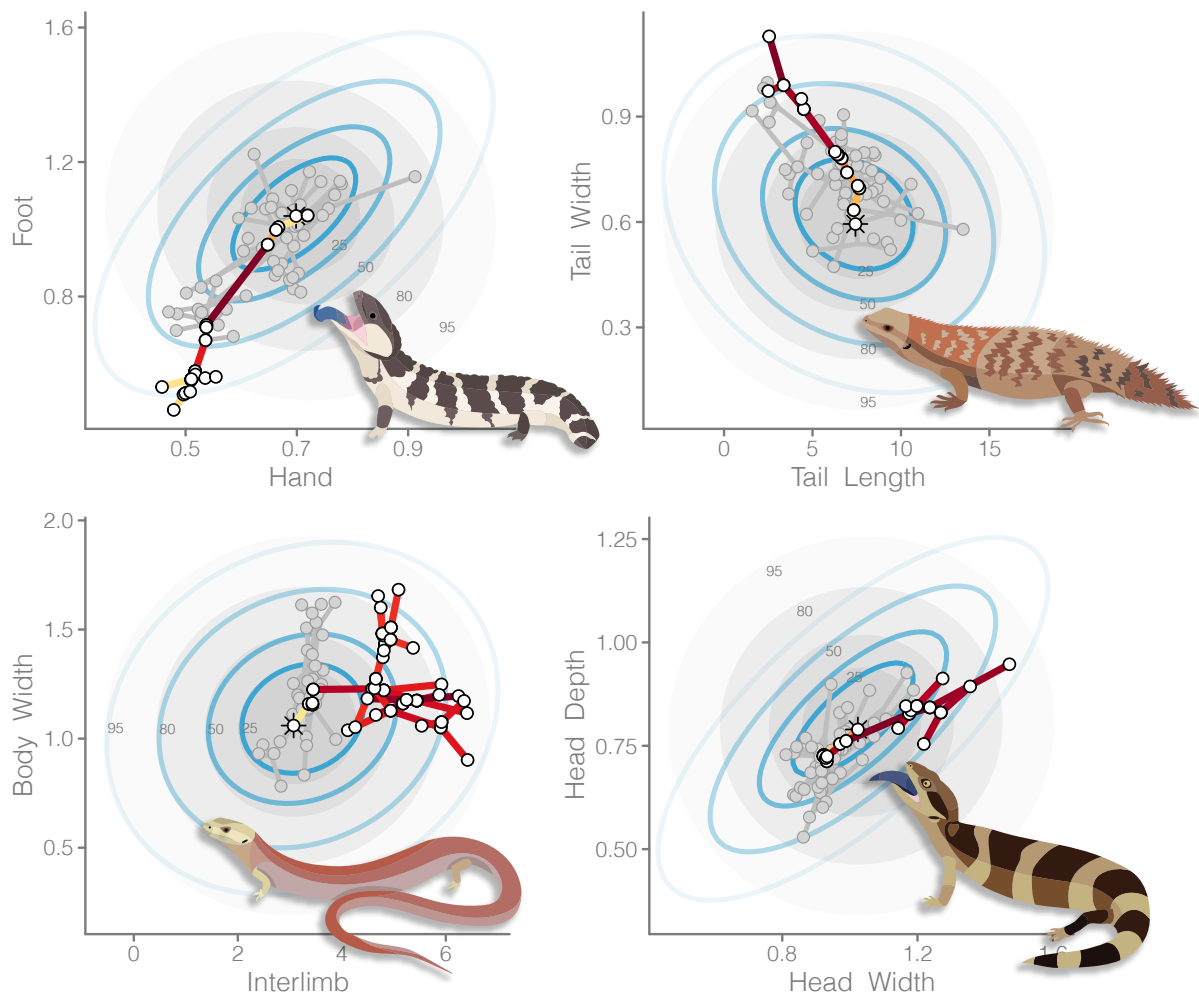


Figure 5: Novel morphologies exceed expectations of uncorrelated trait evolution. Bivariate plots show a phylomorphospace (species points connected by a phylogeny) of the Tiliquini. Each plot isolates a single clade within the group to highlight morphological extremes. Branches of the highlighted clade are colored according to evolutionary rates, with remaining species and branches in grey. In the background are ellipses containing 25/50/80/95% of traits simulated under empirical rates for uncorrelated (grey) and correlated (blue rings) Brownian Motion. Highlighted clades are (clockwise from top left: *Tiliqua*; *Egernia stokesii*–*E.hosmeri*, *Tiliqua rugosa*–*T.gigas*, *Cyclodomorphus*–*Tiliqua*).

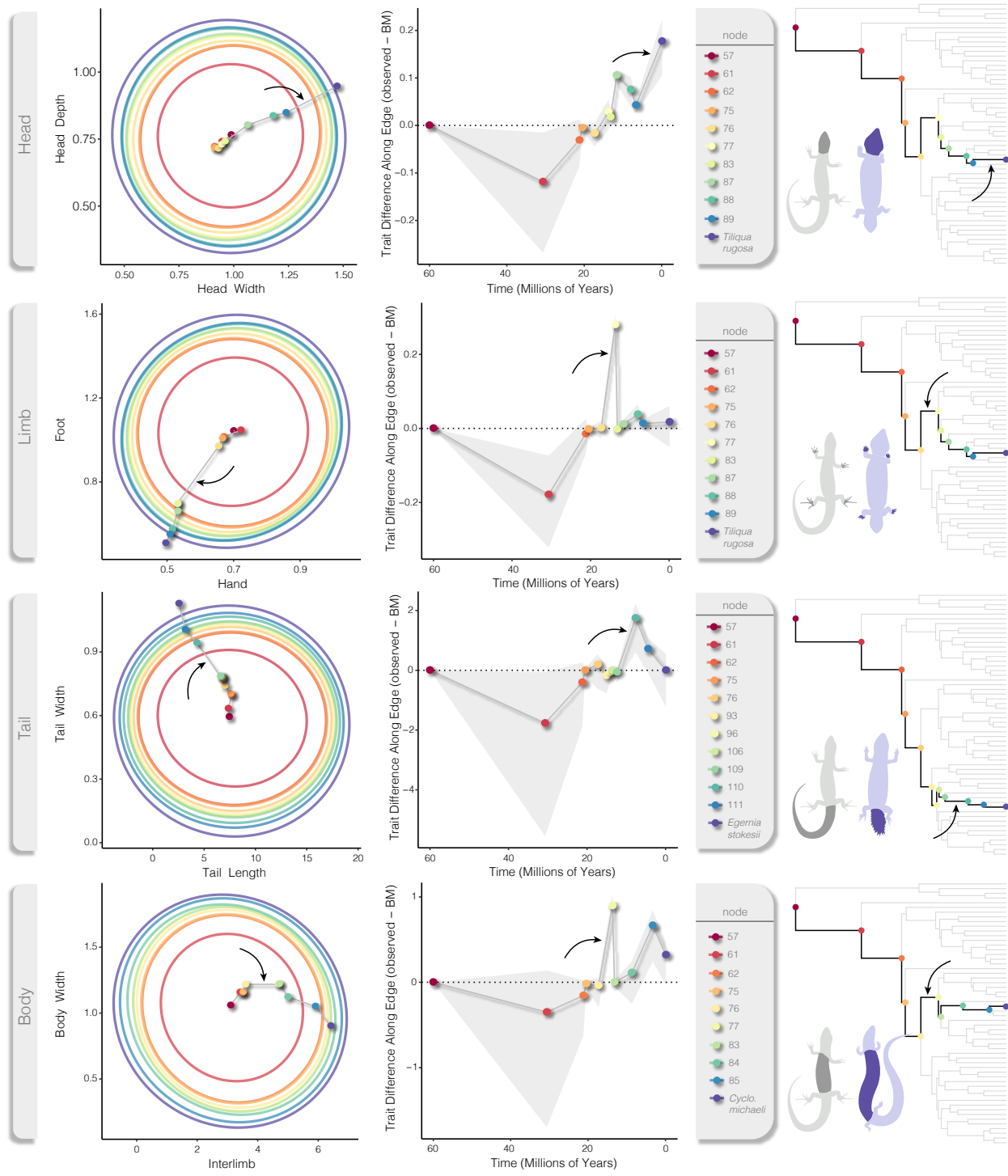


Figure 6: Phenotypic jumps caption below.

Figure 6. Phenotypic jumps are visible as greater than expected trait changes along branches, as estimated under the Variable Rates model and compared to Brownian Motion. Rows correspond to morphological modules, noted in grey at far left. Both circular (left column) and line plots (center column) show the evolutionary trajectory of focal traits from the root of the Tiliquinia

tree (node 57, dark red) to a single tip (dark purple) that has exhibited one or more rate bursts. (left) Large colored rings represent the simulated distribution of trait values under uncorrelated Brownian Motion at each node along the root-to-tip trajectory. Small colored points represent observed and ancestral trait values as estimated under Variable Rates as they traverse the path
350 root-to-tip connected by a grey line. (center) The line plot indicates the trait difference of nodes as (observed - simulated) values with 95% quantiles shown in light grey. Nodes that fall above the dotted line (0) show greater than expected trait change along the branch that leads to that node, visible as greater distances between points in the plots at left. Nodes falling below the dotted line show less trait change than expected. Trees at right serve as a guide for the root-to-tip path of
355 each example, with nodes colored accordingly. Examples of divergent morphologies are illustrated (purple) against a ‘typical’ Tiliquine skink (*Liopholis*—grey). Black arrows in each row indicate the greatest jump in phenotype compared to expectations. References to node numbers can be seen in Fig. S19.

Materials and Methods

360 Walkthroughs of the data, code, analyses, and results are currently available in the *Supplementary Material* on GitHub at www.github.com/IanGBrennan/Tiliquini.

Data Collection

We assembled an exon-capture dataset across 77 Tiliquini skinks representing 48 of 62 currently recognized species, with a focus on Australian taxa (45 of 48 spp.). This sampling
365 covers all 8 genera, as well as many recognized subspecies ([Table S1](#)). We included outgroup representatives from all subfamilies and most tribes, generated as part of broader look at squamate phylogenetics³⁶. Nuclear exons were targeted and sequenced using the Anchored Hybrid Enrichment approach⁴⁹, and resulted in 379 loci (average coverage 367 loci, min = 362, max = 375) totaling ~600 kbp per sample ([Fig.S2](#)). Rough alignments were compiled using MAFFT⁵⁰ and refined using MACSE⁵¹, alignment parameters are specified in
370 the supplementary materials. Per locus information content is summarized in [Fig.S3](#).

We collected 21 linear measurements for 61 Tiliquini skink species from 650 museum samples (average 10 per spp., min.=2, max.=134). These linear measurements aimed to capture the gross morphology of the lizard body plan and are distributed across the head,
375 body, limbs, and tail ([Fig.S4](#)). From the initial 21 measurements some were further divided (e.g. snout-vent length) or dropped to arrive at a set of 19 non-overlapping morphological traits that are summarized in the Supplemental Material ([Morphological Measurements](#)).

Phylogenetic Analyses

We reconstructed individual genealogies for our exon-capture data (n=379) under maximum-likelihood in IQ-TREE 2⁵², allowing the program to assign the best fitting model of molecular evolution using ModelFinder⁵³, then perform 1,000 ultrafast bootstraps⁵⁴. We then estimated the species tree using the shortcut coalescent method ASTRAL III⁵⁵, with IQ-TREE gene trees as input. For comparison we estimated a locus-partitioned concatenated species tree in IQ-TREE. To estimate divergence times among taxa we applied a series of fossil and
380 secondary calibrations in MCMCTree⁵⁶ as outlined in [Table S2](#). We started by concatenating all exonic loci and partitioning them into two partitions, first and second codons together, and third codons separately, then used *baseml*⁵⁷ to get the approximate likelihoods before running *mcmcTree* on the gradient and Hessian (in.BV file) for four replicate analyses. We compared mcmc files for stationarity and convergence, combined them using logCombiner,
385 and used this combined mcmc file to summarize divergence times on our tree (*print* = -1 in .ctl file).

Phenotypic Analyses

Our interest is in identifying the tempo and mode of evolution that produces morphological novelty and so we focus on the dynamics of morphological diversification in the Tiliquini radiation. Our approach is based on a novel dataset that summarizes the lizard body plan.
395 We started by generating mean trait values per species and removed the effect of absolute

size by transforming our trait values into log-shape ratios. To identify independently evolving morphological modules we designed module models that ranged from highly specialized (head, limbs, body, and tail traits evolve independently) to highly integrated (null model in which all traits belong to a single module), see Supplementary Material for details. We compared model likelihoods and estimated correlation coefficients using *EMMLi*²⁸ and used the preferred model to designate module-specific datasets.

To identify the evolutionary mode of individual morphological traits we fit a series of models ranging from a basic unbiased random walk to entirely punctuated. These allowed phenotypes to evolve through incremental change (Brownian Motion—BM), incremental change around an optimum (Ornstein Uhlenbeck), decreasing change with time (Early Burst)—akin to an adaptive radiation scenario, two “pulse” or “jump” models which allow change in instantaneous bursts (Jump Normal, Normal Inverse Gaussian), and a Variable Rates model in which rates of change vary across individual branches of the tree—similar to the relaxed clock model of timetree estimation. For consistency we fit the BM, OU, EB, JN, and NIG models in *pulsR*²¹. We fit the VR model in *Bayes Traits V3*⁵⁸ and processed the output using the standalone *PPPostProcess* software. We compared model fit by AIC scores. *Bayes Traits* implements an MCMC algorithm so to estimate a maximum likelihood for the VR model we transformed the input tree by the estimated median rate scalar, then fit the observed data to the transformed tree using BM in *pulsR*. We obtained an AIC value by penalizing the likelihood for each scaled branch of the transformed tree with mean scalar r greater than two, in addition to the estimation of the rate parameter and root state. We then calculated AICw for each model and identified a preferred model if its AICw was greater than twice the next best model.

To understand the temporal and phylogenetic heterogeneity of evolution we estimated ancestral states for each trait under the rate heterogeneous VR model by optimizing Brownian Motion on the VR rate-transformed trees in *phytools*⁵⁹. We extrapolated trait values linearly along branches given start and end values at nodes and a constant evolutionary rate. We did this from the root to the tips in 0.1 million year windows across all branches. To summarize the standing morphological variation across the same temporal windows we calculated disparity as both the variance and the average squared Euclidean distance among all pairs of contemporaneous taxa. Similarly we extracted the mean evolutionary rate in 0.1 million year windows for each trait and module. To determine if our observed patterns follow a null expectation of the accumulation of disparity through time we simulated univariate and uncorrelated and correlated multivariate datasets for each trait and module applying parameter estimates from observed data for theta, sigma, and covariance. We carried out the same disparity and rate through time extraction methods in 0.1 million year windows. To understand the relative contribution of niche expansion and niche packing to the accumulation of disparity through time we compared slopes of the accumulation of variance of observed traits and modules to simulated data. We plotted the trends in variance, rate, and slopes using custom functions found in the scripts included in the supplement.

Lastly, to summarize the major avenues of morphological change we ran PCA on (1) all traits jointly and across (2) individual modules and (3) clades separately, then fit linear models to the first 2 PC axes (always accounting for $\geq 90\%$ of variance). This allowed us to identify the major axes of elaboration (PC1) and innovation (PC2) following the language of¹² and¹³. Tracking the angle (slope of regression) and extent of trait change between individual

nodes enabled us to qualitatively identify periods of primarily innovation or elaboration on a branch-by-branch basis.

References

- 445 1. Foote, M. (1997). The evolution of morphological diversity. *Annual Review of Ecology and Systematics* *28*, 129–152.
2. Deline, B., Greenwood, J.M., Clark, J.W., Puttick, M.N., Peterson, K.J., and Donoghue, P.C. (2018). Evolution of metazoan morphological disparity. *Proceedings of the National Academy of Sciences* *115*, E8909–E8918.
- 450 3. Lynch, M. (1990). The rate of morphological evolution in mammals from the stand-point of the neutral expectation. *The American Naturalist* *136*, 727–741.
4. Hansen, T.F., and Houle, O. (2004). Evolvability, stabilizing selection, and the problem. *Phenotypic integration: Studying the ecology and evolution of complex phenotypes*, 130.
5. Hall, B.K. (1996). Bauplane, phylotypic stages, and constraint-why there are so few types of animals. *Evolutionary Biology*, Vol *29* *29*, 215–261.
- 455 6. Vermeij, G.J. (2015). Forbidden phenotypes and the limits of evolution. *Interface Focus* *5*, 20150028.
7. Galis, F., Metz, J.A., and Alphen, J.J. van (2018). Development and evolutionary constraints in animals. *Annual Review of Ecology, Evolution, and Systematics* *49*, 499–522.
- 460 8. Arnold, S.J., Pfrender, M.E., and Jones, A.G. (2001). The adaptive landscape as a conceptual bridge between micro-and macroevolution. *Microevolution rate, pattern, process*, 9–32.
9. Hansen, T.F., and Martins, E.P. (1996). Translating between microevolutionary process and macroevolutionary patterns: The correlation structure of interspecific data. *Evolution* *50*, 1404–1417.
10. Felsenstein, J. (1988). Phylogenies and quantitative characters. *Annual Review of Ecology and Systematics* *19*, 445–471.
- 465 11. Schlüter, D. (1996). Ecological causes of adaptive radiation. *The American Naturalist* *148*, S40–S64.
12. Endler, J.A., Westcott, D.A., Madden, J.R., and Robson, T. (2005). Animal visual systems and the evolution of color patterns: Sensory processing illuminates signal evolution. *Evolution* *59*, 1795–1818.
- 470 13. Guillerme, T., Bright, J.A., Cooney, C.R., Hughes, E.C., Varley, Z.K., Cooper, N., Beckerman, A.P., and Thomas, G.H. (2023). Innovation and elaboration on the avian tree of life. *bioRxiv*, 2022–2008.
14. Simpson, G.G. (1944). *Tempo and mode in evolution* (Columbia University Press).
15. Hunt, G. (2008). Gradual or pulsed evolution: When should punctuational explanations be preferred? *Paleobiology* *34*, 360–377.
- 475 16. Hunt, G., Hopkins, M.J., and Lidgard, S. (2015). Simple versus complex models of trait evolution and stasis as a response to environmental change. *Proceedings of the National Academy of Sciences* *112*, 4885–4890.

- 480
17. Venditti, C., Meade, A., and Pagel, M. (2011). Multiple routes to mammalian diversity. *Nature* *479*, 393–396.
 18. Uyeda, J.C., Hansen, T.F., Arnold, S.J., and Pienaar, J. (2011). The million-year wait for macroevolutionary bursts. *Proceedings of the National Academy of Sciences* *108*, 15908–15913.
 19. Landis, M.J., Schraiber, J.G., and Liang, M. (2013). Phylogenetic analysis using lévy processes: Finding jumps in the evolution of continuous traits. *Systematic biology* *62*, 193–204.
 20. Baker, J., Meade, A., Pagel, M., and Venditti, C. (2016). Positive phenotypic selection inferred from phylogenies. *Biological Journal of the Linnean Society* *118*, 95–115.
 - 485 21. Landis, M.J., and Schraiber, J.G. (2017). Pulsed evolution shaped modern vertebrate body sizes. *Proceedings of the National Academy of Sciences* *114*, 13224–13229.
 22. Bastide, P., and Didier, G. (2023). The cauchy process on phylogenies: A tractable model for pulsed evolution. *bioRxiv*, 2023–2004.
 23. Matthew, W.D. (1914). Time ratios in the evolution of mammalian phyla. A contribution to the problem of the age of the earth. *Science* *40*, 232–235.
 - 490 24. Chapple, D.G. (2003). Ecology, life-history, and behavior in the australian scincid genus egernia, with comments on the evolution of complex sociality in lizards. *Herpetological Monographs* *17*, 145–180.
 25. Gardner, M.G., Hugall, A.F., Donnellan, S.C., Hutchinson, M.N., and Foster, R. (2008). Molecular systematics of social skinks: Phylogeny and taxonomy of the egernia group (reptilia: scincidae). *Zoological Journal of the Linnean Society* *154*, 781–794.
 - 495 26. Thorn, K., Hutchinson, M., Lee, M., Brown, N., Camens, A., and Worthy, T. (2021). A new species of proegernia from the namba formation in south australia and the early evolution and environment of australian egerniine skinks. *Royal Society Open Science* *8*, 201686.
 27. Linkem, C.W., Minin, V.N., and Leaché, A.D. (2016). Detecting the anomaly zone in species trees and evidence for a misleading signal in higher-level skink phylogeny (squamata: scincidae). *Systematic biology* *65*, 465–477.
 - 500 28. Goswami, A., and Finarelli, J.A. (2016). EMMLi: A maximum likelihood approach to the analysis of modularity. *Evolution* *70*, 1622–1637.
 29. Imfeld, T.S., and Barker, F.K. (2022). Songbirds of the americas show uniform morphological evolution despite heterogeneous diversification. *Journal of evolutionary biology* *35*, 1335–1351.
 30. Sallan, L.C., and Friedman, M. (2012). Heads or tails: Staged diversification in vertebrate evolutionary radiations. *Proceedings of the Royal Society B: Biological Sciences* *279*, 2025–2032.
 - 505 31. Gardner, M.G., Pearson, S.K., Johnston, G.R., and Schwarz, M.P. (2016). Group living in squamate reptiles: A review of evidence for stable aggregations. *Biological Reviews* *91*, 925–936.

32. Thorn, K.M., Hutchinson, M.N., Archer, M., and Lee, M.S. (2019). A new scincid lizard from the miocene of northern australia, and the evolutionary history of social skinks (scincidae: egerniinae). *Journal of Vertebrate Paleontology* *39*, e1577873.
33. Thorn, K.M., Fusco, D.A., Hutchinson, M.N., Gardner, M.G., Clayton, J.L., Prideaux, G.J., and Lee, M.S. (2023). A giant armoured skink from australia expands lizard morphospace and the scope of the pleistocene extinctions. *Proceedings of the Royal Society B* *290*, 20230704.
- 510 34. Chapple, D.G., Keogh, J.S., and Hutchinson, M.N. (2004). Molecular phylogeography and systematics of the arid-zone members of the egernia whitii (lacertilia: Scincidae) species group. *Molecular phylogenetics and evolution* *33*, 549–561.
35. Chapple, D.G., and Keogh, J.S. (2006). Group structure and stability in social aggregations of white's skink, egernia whitii. *Ethology* *112*, 247–257.
- 515 36. Burbrink, F.T., Grazziotin, F.G., Pyron, R.A., Cundall, D., Donnellan, S., Irish, F., Keogh, J.S., Kraus, F., Murphy, R.W., Noonan, B., et al. (2020). Interrogating genomic-scale data for squamata (lizards, snakes, and amphisbaenians) shows no support for key traditional morphological relationships. *Systematic biology* *69*, 502–520.
37. Novack-Gottshall, P.M., Sultan, A., Smith, N.S., Purcell, J., Hanson, K.E., Lively, R., Ranjha, I., Collins, C., Parker, R., Sumrall, C.D., et al. (2022). Morphological volatility precedes ecological innovation in early echinoderms. *Nature Ecology & Evolution* *6*, 263–272.
- 520 38. Leslie, A.B., Simpson, C., and Mander, L. (2021). Reproductive innovations and pulsed rise in plant complexity. *Science* *373*, 1368–1372.
39. Hansen, T.F. (1997). Stabilizing selection and the comparative analysis of adaptation. *Evolution* *51*, 1341–1351.
40. Beaulieu, J.M., Jhueng, D.-C., Boettiger, C., and O'Meara, B.C. (2012). Modeling stabilizing selection: Expanding the ornstein–uhlenbeck model of adaptive evolution. *Evolution* *66*, 2369–2383.
- 525 41. Burin, G., Park, T., James, T.D., Slater, G.J., and Cooper, N. (2023). The dynamic adaptive landscape of cetacean body size. *Current Biology* *33*, 1787–1794.
42. Gould, S.J., and Eldredge, N. (1972). Punctuated equilibria: An alternative to phyletic gradualism. *Models in paleobiology* *1972*, 82–115.
43. Malmgren, B.A., Berggren, W.A., and Lohmann, G. (1983). Evidence for punctuated gradualism in the late neogene globorotalia tumida lineage of planktonic foraminifera. *Paleobiology* *9*, 377–389.
- 530 44. Pagel, M., O'Donovan, C., and Meade, A. (2022). General statistical model shows that macroevolutionary patterns and processes are consistent with darwinian gradualism. *Nature communications*, 1113.
45. Cooney, C.R., Bright, J.A., Capp, E.J., Chira, A.M., Hughes, E.C., Moody, C.J., Nouri, L.O., Varley, Z.K., and Thomas, G.H. (2017). Mega-evolutionary dynamics of the adaptive radiation of birds. *Nature* *542*, 344–347.

- 535 46. Ronco, F., Matschiner, M., Böhne, A., Boila, A., Büscher, H.H., El Taher, A., Indermaur, A., Malinsky, M., Ricci, V., Kahmen, A., et al. (2021). Drivers and dynamics of a massive adaptive radiation in cichlid fishes. *Nature* *589*, 76–81.
47. Alho, J., Herczeg, G., Laugen, A., Räsänen, K., Laurila, A., and Merilä, J. (2011). Allen’s rule revisited: Quantitative genetics of extremity length in the common frog along a latitudinal gradient. *Journal of evolutionary biology* *24*, 59–70.
48. Ramm, T., Roycroft, E.J., and Müller, J. (2020). Convergent evolution of tail spines in squamate reptiles driven by microhabitat use. *Biology Letters* *16*, 20190848.
- 540 49. Lemmon, A.R., Emme, S.A., and Lemmon, E.M. (2012). Anchored hybrid enrichment for massively high-throughput phylogenomics. *Syst Biol* *61*, 727–744. [10.1093/sysbio/sys049](https://doi.org/10.1093/sysbio/sys049).
50. Katoh, K., and Standley, D.M. (2013). MAFFT multiple sequence alignment software version 7: Improvements in performance and usability. *Molecular biology and evolution* *30*, 772–780.
- 545 51. Ranwez, V., Douzery, E.J., Cambon, C., Chantret, N., and Delsuc, F. (2018). MACSE v2: Toolkit for the alignment of coding sequences accounting for frameshifts and stop codons. *Molecular biology and evolution* *35*, 2582–2584.
52. Minh, B.Q., Schmidt, H.A., Chernomor, O., Schrempf, D., Woodhams, M.D., Von Haeseler, A., and Lanfear, R. (2020). IQ-TREE 2: New models and efficient methods for phylogenetic inference in the genomic era. *Molecular biology and evolution* *37*, 1530–1534.
53. Kalyaanamoorthy, S., Minh, B.Q., Wong, T.K., Von Haeseler, A., and Jermiin, L.S. (2017). ModelFinder: Fast model selection for accurate phylogenetic estimates. *Nature methods* *14*, 587–589.
- 550 54. Haeseler, A. von, Minh, B.Q., and Nguyen, M.A.T. (2013). Ultrafast approximation for phylogenetic bootstrap. *Molecular Biology and Evolution* *30*, 1188–1195. [10.1093/molbev/mst024](https://doi.org/10.1093/molbev/mst024).
- 55 55. Zhang, C., Sayyari, E., and Mirarab, S. (2017). ASTRAL-III: Increased scalability and impacts of contracting low support branches. *53–75*.
56. Rannala, B., and Yang, Z. (2007). Inferring speciation times under an episodic molecular clock. *Systematic biology* *56*, 453–466.
57. Reis, M. dos, and Yang, Z. (2011). Approximate likelihood calculation on a phylogeny for bayesian estimation of divergence times. *Molecular biology and evolution* *28*, 2161–2172.
58. Venditti, C., Meade, A., and Pagel, M. (2011). Multiple routes to mammalian diversity. *Nature* *479*, 393–396.
- 560 59. Revell, L.J. (2012). Phytools: An r package for phylogenetic comparative biology (and other things). *Methods in ecology and evolution*, 217–223.

Appendix

Taxonomic Implications and Changes

- 565 As a result of our phylogenetic investigation, some taxonomic issues must be addressed and others will unfortunately remain outstanding until more focused sampling can be achieved. We comment on both cases below.

(1) Paraphyly of *Lissolepis*: Phylogenetic estimation and topology testing do not support 570 the monophyly of *Lissolepis*. The type species of *Lissolepis* is *L.luctuosa* (Peters 1866), and despite *L.coventryi* (Storr 1978) forming a clade with *Liopholis*, these taxa are morphologically distinct. We feel that to acknowledge the distinctiveness of *L.coventryi* the best course of action is to erect a new genus to contain this species.

Paluarius gen. nov. Brennan, Chapple, Keogh & Donnellan

575 *Egernia* Storr 1978

Lissolepis Gardner 2008

Type species: *Egernia coventryi* Storr 1978

Diagnosis and definition: Currently a monotypic genus comprising a single medium sized 580 ($\bar{x} = 80$ mm; max = 100 mm) skink with four well developed limbs each with five digits and fourth toe much longer than third. Lower eyelid movable and without a transparent ‘window’. Parietal and nasal scales both narrowly separated. Ear aperture small and with two anterior lobules. Distinguished from *Lissolepis* by broad geographic separation (southwest WA for *Lis.*; extreme southeast SA and coastal VIC for *Pal.*), continuous striped (*Paluarius*) rather than spotty (*Lissolepis*) dorsal patterning, shorter and blunter head (head length 15% of 585 SVL in *Pal.*, 20% in *Lis.*), fewer midbody scale rows, longer postnasal crease that runs to the top of the nasal scale, and smaller size (80–100 mm vs. 100–129mm).

Etymology: This skink lives among swamps, heaths, and marshes in far southeastern Australia. In allusion to its preferred habitat, from latin ‘palus’—swamp and ‘-arius’—where things are kept, together meaning ‘keeper of the swamp’.

590 Contents: *Paluarius coventryi* comb. nov. (Storr 1978)

(2) Paraphyly of *Cyclodomorphus*: Phylogenetic estimates and topology testing do not support the monophyly of *Cyclodomorphus* (Fitzinger 1843). The type species of *Cyclodomorphus* is *C. casuarinae* (Dumeril & Bibron 1839), which along with the species 595 *gerrardii*, *michaeli*, and *praealtus* form a clade with *Tiliqua*. We propose a new generic name to contain the taxa more closely related to *C. maximus* than to *C. gerrardii*.

Caeruleulus gen. nov. Brennan, Chapple, Keogh & Donnellan

Cyclodus Dumeril & Bibron 1839

Hinula Gunther 1867

600 *Lygosoma* Hardwicke & Gray 1828

Tiliqua Gray 1825

Omolepida Gray 1845

Cyclodomorphus Fitzinger 1843

Type species: *Omolepida maxima* Storr 1976

605 Diagnosis and definition: A genus of moderate to large, elongate skinks characterized

by long interlimb (trunk) lengths and relatively short limbs, each with five digits. Many scalation characters are shared with *Cyclodomorphus*, and so make distinguishing the two difficult. Starting from the snout, nasals are in contact with one another and broadly contact the frontonasal which widely separates the prefrontals. There are no subocular scales, but 610 three supraocular scales, the anterior two of which contact the frontal. Eyelid movable and no transparent ‘window’. Parietal scales are widely separated by an interparietal scale. Ear opening small, with small anterior lobules (usually 2).

Etymology: From the Latin ‘caeruleus’ for blue and the diminutive ‘-ulus’, meaning ‘little blue one’, alluding to their blue tongues and smaller size relative to the larger ‘bluetongue’ 615 relatives *Tiliqua*.

Contents: *Caeruleulus branchialis* comb. nov. (Gunther 1867); *Caeruleulus celatus* comb. nov. (Shea & Miller 1995); *Caeruleulus maximus* comb. nov. (Storr 1976); *Caeruleulus melanops elongatus* comb. nov. (Shea & Miller 1995); *Caeruleulus melanops melanops* comb. nov. (Stirling & Zietz 1893); *Caeruleulus melanops siticulosus* comb. nov. (Shea & 620 Miller 1995); *Caeruleulus venustus* comb. nov. (Shea & Miller 1995).

Comment: Wells (2007) proposed splitting *Cyclodomorphus*, reallocating *C. gerrardii* to *Hemisphaeriodon* and creating a new generic name for the *Cyclodomorphus maximus* clade. In following the best practices in herpetological nomenclature outlined by Kaiser et al. (2013) 625 and adopted by the Australian Society of Herpetologists in their Position Statement on Taxonomy (2022) we do not recognize the name proposed by Wells (2007) and instead provide *Caeruleulus* as the generic name for this clade of tiliquine skinks.

(3) *Cyclodomorphous melanops*: Our limited sampling suggests species-level divergences among the three subspecies of *C. melanops* (~4mya, 2mya), however unpublished mtDNA 630 data shows more complicated genetic history among these taxa and the closely related *C. venustus*, *C. celatus*, and the currently unsampled *C. branchialis*. In light of these results we take the conservative stance of retaining the subspecies as is, and suggest a more focused study with greater sampling would provide better understanding of this morphologically conservative clade.

635 (4) *Egernia stokesii*: Similarly, the divergence between *E. stokesii* subspecies *E.s.badia* and *E.s.zellingi* are comparatively deep (~4.5mya), and subspecies are recovered as reciprocally monophyletic. However, our sampling lacks representatives of the nominate subspecies *E.s.stokesii*. Unpublished mtDNA data does not appear to distinguish between subspecies 640 *E.s.stokesii* and *E.s.badia*, and so we refrain from making taxonomic changes without having *E.s.stokesii* included in our analyses.

(5) Paraphyly of *Liopholis inornata*: Our sampling of *L. inornata* and sister taxa *L. slateri* and *L. sp. nov.* from Purnululu highlight a complicated phylogenetic history. As currently understood, *L. inornata* is a wide ranging species found across much of arid WA, SA, NSW, and QLD. This range overlaps entirely with *L. slateri* with which it could potentially be confused, but remains allopatric from *L. sp. nov.* Purnululu. We highlight this clade as 645 a group which needs a much more thorough population genetic assessment to resolve.

650 (6) Paraphyly of *Liopholis margaretae*: Chapple & Keogh (2004) identified the non-

monophyly of *Liopholis margaretae* subspecies and recommended that *L. personata* be identified as a distinct species. Despite this, sources such as the [Reptile Database](#) and [Atlas of Living Australia](#) continue to treat these taxa as conspecific. Our phylogenetic analyses are concordant with those of Chapple & Keogh (2004) and we echo the evolutionary distinctiveness of *Liopholis personata* as a species.

655

Supplementary Material

Supplementary material included below consists of additional figures, tables, and extended methods to complement the main text.

Table S1. Taxon sampling for this project.

Genus	Species	Subspecies	Specimen Registration	ABTC No.	Locality	State	Country	Latitude	Longitude
Bellatorias	frerei	—	AMS R.113970	10881	Bunya Mountains	QLD	Australia		
Bellatorias	frerei	—	AMS R.96317	11439	Heathlands	QLD	Australia		
Bellatorias	major	—	SAMA R33412	4115	Whian Whian SF	NSW	Australia		
Bellatorias	obiri	—	AMS R.100018	11440	Jabiluka	NT	Australia		
Corucia	zebrata	—	—	50418	Levaleva Choiseul Island	—	Solomon Islands		
Cyclodomorphus	melanops	elongatus	MAGNT R20662	29413	Finke Gorge NP	NT	Australia		
Cyclodomorphus	casuarinae	—	SAMA R22957	54924	Mount Victoria	NSW	Australia		
Cyclodomorphus	casuarinae	—	SAMA R63333	101476	—	TAS	Australia		
Cyclodomorphus	celatus	—	SAMA R22873	54920	Burns Beach	WA	Australia		
Cyclodomorphus	gerrardii	—	SAMA R34884	16792	Paluma	QLD	Australia		
Cyclodomorphus	maximus	—	WAM R168816	135574	Middle Osborn Island	WA	Australia		
Cyclodomorphus	melanops	siticulosus	SAMA R52374	58905	St. Francis Island	SA	Australia		
Cyclodomorphus	melanops	melanops	SAMA R34056	11739	Mount Stuart Homestead	WA	Australia		
Cyclodomorphus	praecaltus	—	—	97283	Bogong High Plains	VIC	Australia		
Cyclodomorphus	venustus	—	SAMA R18869	54897	Port Germein Dump	SA	Australia		
Egernia	cunninghami	—	AMS R.112873	11398	Yetman	NSW	Australia		
Egernia	cunninghami	—	AMS R.118939	14392	Kanangra Walls	NSW	Australia		
Egernia	depressa	—	SAMA R22856	53933	Python Pool	WA	Australia		
Egernia	depressa	—	WAM R120631	63425	Mardathuna	WA	Australia		
Egernia	douglasi	—	ABTC 141482	141482	Beverley Springs Homestead	WA	Australia		
Egernia	eos	—	WAM R98079	23913	Ainsley Gorge	WA	Australia		
Egernia	episodus	—	WAM R90897	63515	Woodstock	WA	Australia		
Egernia	formosa	—	SAMA R29267	53997	Yalgo	WA	Australia		
Egernia	formosa	—	WAM R103993	61869	Woodstock Station	WA	Australia		
Egernia	hosmeri	—	SAMA R36707	17065	Mount Isa	QLD	Australia		
Egernia	kingii	—	SAMA R29444	54006	Mount Clarence	WA	Australia		
Egernia	napoleonis	—	SAMA R23080	53949	Denmark	WA	Australia		
Egernia	pilbarensis	—	WAM R132519	63479	Burrup Peninsula	WA	Australia		
Egernia	richardi	—	SAMA R26315	40639	Koonalda Station	SA	Australia		
Egernia	richardi	—	SAMA R63272	112886	Merdayerah Sandpatch	SA	Australia		
Egernia	rugosa	—	—	108820	Charleville	QLD	Australia		
Egernia	rugosa	—	—	108823	Charleville	QLD	Australia		
Egernia	saxatilis	intermedia	SAMA R44004	12812	The Grampians	VIC	Australia		
Egernia	stokesii	zellingi	SAMA R42897	9143	Stonehenge	QLD	Australia		
Egernia	stokesii	zellingi	SAMA R45053	35026	Toopawarinna Hill	SA	Australia		
Egernia	stokesii	zellingi	SAMA R44127	57871	Pernatty Station	SA	Australia		
Egernia	stokesii	badia	WAM R135193	63511	Walycatchem	WA	Australia		
Egernia	stokesii	badia	WAM R152997	92933	Walga Rock	WA	Australia		
Egernia	stokesii	badia	WAM R152998	92934	Walga Rock	WA	Australia		
Egernia	striolata	—	AMS R.126116	1150	Denham	NSW	Australia		
Egernia	striolata	—	SAMA R53262	70470	Telowie	SA	Australia		
Egernia	striolata	—	SAMA R55661	76988	Moorrinya NP	QLD	Australia		
Egernia	striolata	—	QM J86594	100573	Durikai SF	QLD	Australia		

Genus	Species	Subspecies	Specimen Registration	ABTC No.	Locality	State	Country	Latitude	Longitude
Eutropis	longicaudata	—	SAMA R38916	57273	—	—	Malaysia		
Liopholis	guthega	—	SAMA R37781	16273	Kosciusko NP	NSW	Australia		
Liopholis	inornata	—	MAGNT R20673	29437	Finke Gorge NP	NT	Australia		
Liopholis	inornata	—	SAMA R45219	58081	Mootatunga	SA	Australia		
Liopholis	inornata	—	SAMA R49140	58604	Eyre Peninsula	SA	Australia		
Liopholis	inornata	—	NMV D65868	61607	Buningonia Springs	WA	Australia		
Liopholis	kintorei	—	WAM R131047	63449	—	WA	Australia		
Liopholis	margaretae	margaretae	SAMA R51590	42404	Amata	SA	Australia		
Liopholis	margaretae	personata	SAMA R24815	53965	Mount Remarkable NP	SA	Australia		
Liopholis	modesta	—	SAMA R39172	12411	Retreat	NSW	Australia		
Liopholis	montana	—	SAMA R37768	16389	Mount Gingera	ACT	Australia		
Liopholis	multiscutata	—	SAMA R63458	126142	—	SA	Australia		
Liopholis	pulchra	pulchra	WAM R132054	63464	D'Entrecasteaux NP	WA	Australia		
Liopholis	sp. nov.	—	WAM R156715	85105	Purnululu NP	WA	Australia		
Liopholis	slateri	slateri	—	99920	Finke River	NT	Australia	-23.8142	132.6636
Liopholis	striata	—	SAMA R45402	58180	Ampeinna Hills	SA	Australia		
Liopholis	whitii	—	SAMA R53588	94846	Spring Mount	SA	Australia		
Lisssolepis	coventryi	—	SAMA R45916	58241	Nelson	SA	Australia		
Lisssolepis	luctuosa	—	WAM R90386	135575	Walpole	WA	Australia		
Lisssolepis	luctuosa	—	WAM R90226	135576	Lake Wilson	WA	Australia		
Tiliqua	adelaidensis	—	SAMA R42426	57682	Burra	SA	Australia		
Tiliqua	gigas	gigas	AMS R.124720	48811	Usino	Madang	Papua New Guinea		
Tiliqua	gigas	gigas	AMS R.124721	48812	Usino	Madang	Papua New Guinea		
Tiliqua	gigas	evanescens	AMS R.129710	50170	Guleguleu Normanby Island	Milne Bay	Papua New Guinea		
Tiliqua	multifasciata	—	SAMA R49974	37896	Purni Bore	SA	Australia		
Tiliqua	nigrolutea	—	SAMA R33410	4114	Clarkefield	VIC	Australia		
Tiliqua	occipitalis	—	SAMA R28391	54961	Iron Knob	SA	Australia		
Tiliqua	rugosa	rugosa	SAMA R18978	55216	Bremer Bay	WA	Australia		
Tiliqua	rugosa	aspera	SAMA R20587	55264	Cowell	SA	Australia		
Tiliqua	scincoides	intermedia	QM J51107	24812	Cape Flattery	QLD	Australia		
Tiliqua	scincoides	chimaera	WAM R112258	101416	Latdalam	—	Indonesia		
Tiliqua	scincoides	scincoides	SAMA R28511	54968	Minnipa	SA	Australia		
Tiliqua	scincoides	intermedia	SAMA R53937	70143	Tunnel Creek Gorge	WA	Australia		
Tribolonotus	gracilis	—	AMS R.122119	14359	Karkar Island	—	Papua New Guinea		

660 **Table S2.** Fossil calibrations as implemented in MCMCTree. The root (Mabuyini + Tiliquini) and the Tiliquini crown are
 665 calibrated with Cauchy distributions based on estimates from previous studies. These leave 2.5% of the distribution each above
 and below the minimum and maximum ages noted below. The calibration for the crown of Australian Tiliquini is bounded on
 the lower end by the Dwornamor Local Fauna of Riversleigh which includes *Tiliqua pusilla* and *Egernia gillespieae*, and on the
 the maximum bound. The remaining calibrations are all soft minimums with 2.5% below the minimum.

Node	Fossil Information	Calibration	Split	Source
A	Soft Secondary	'>0.5<0.8'	Root (Mabuyini + Tiliquini) [C	ITE Burbrink et al. 2021; Thorn et al. 2021]
B	Soft Secondary	'>0.37<0.62'	Crown Tiliquini (<i>Tribolonotus</i> + all others) [CITE Thorn et al. 2019; Thorn et al. 2021]
C	<i>Tiliqua pusilla</i> †, <i>Egernia gillespieae</i> †, <i>Proegernia palankarinnensis</i> †, <i>P. mikebulli</i> †	'B(0.15,0.26,0.025,0.2)'	Crown Australian Tiliquini [(<i>Corucia</i> + all others)	CITE Martin et al. 2004; Thorn et al. 2019]
D	<i>Egernia gillespieae</i> †	'>0.15'	Crown <i>Egernia</i>	[CITE Thorn et al. 2019]
E	<i>Tiliqua cf. scincoides</i> †	'>0.036'	<i>Tiliqua gigas</i> + <i>Tiliqua scincoides</i>	[CITE Mackness & Hutchinson 2000]
F	<i>Egernia cf. hosmeri</i> †	'>0.036'	<i>Egernia hosmeri</i> + <i>Egernia stokesii</i>	[CITE Mackness & Hutchinson 2000]

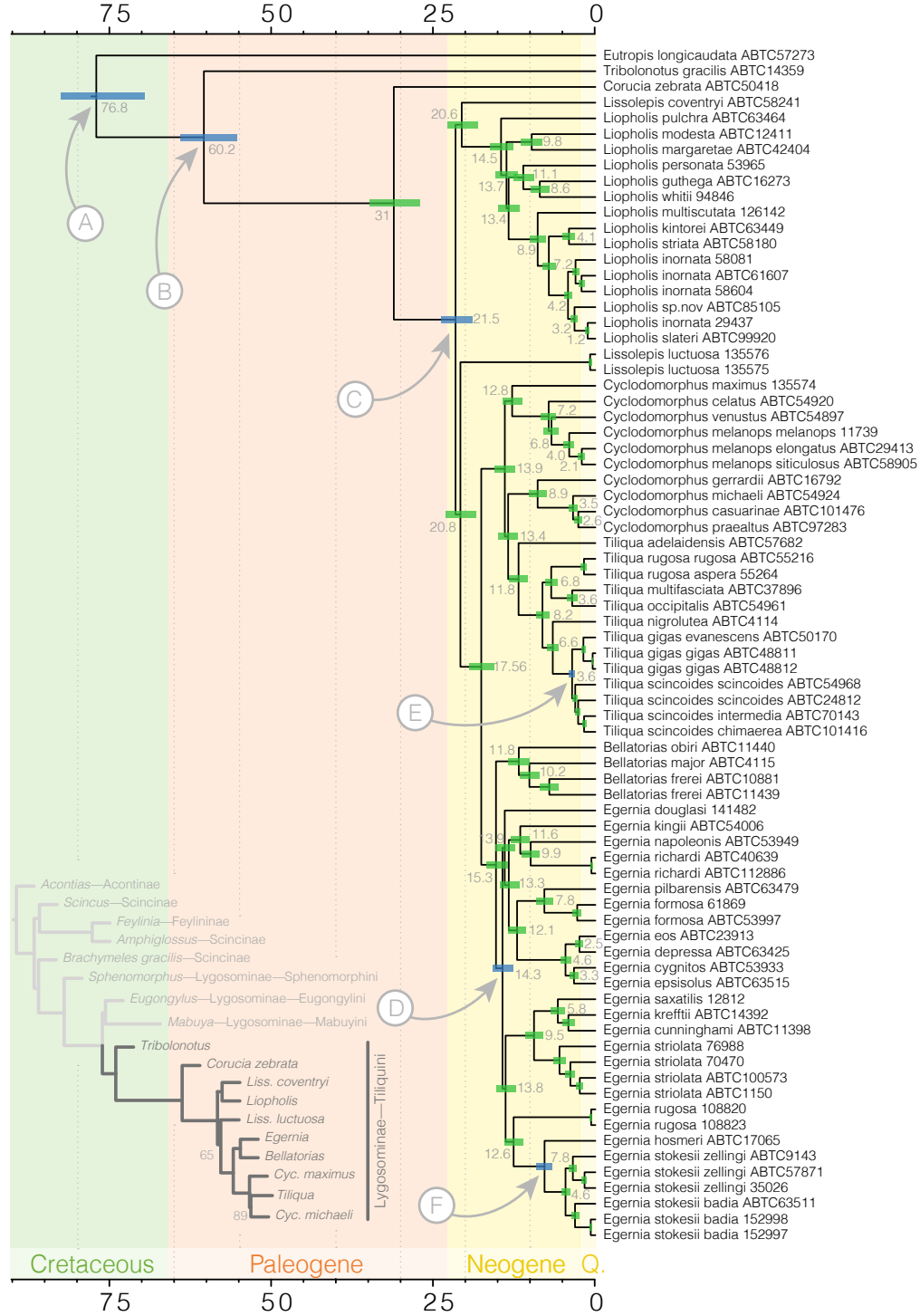


Figure S1: Tiliquini species tree estimated with ASTRAL from IQ-TREE genetrees and time-calibrated with MCMCTree. Shaded bars at nodes indicate 95% confidence estimates on ages. Nodes labelled by letters A–F correspond to fossil calibrations listed in Table S2. Inset tree depicts the scincid phylogeny estimated from AHE data showing the placement of the Tiliquini among the Lygosominae.

Alignment Specifications

Input MAFFT/MUSCLE alignments were refined with MACSE using the following call:

```
$ java -jar /Applications/macse_v2.03.jar \
    -prog refineAlignment -align [rough alignment path] \
    -optim 1 -local_realign_init 0.1 -local_realign_dec 0.1 \
    -fs 10 -stop 10
```

Investigating Data Completeness and Informativeness

Below we visualize data completeness and informativeness on a per sample and per locus basis, as well as provide some insight into our data cleaning and sample selection.

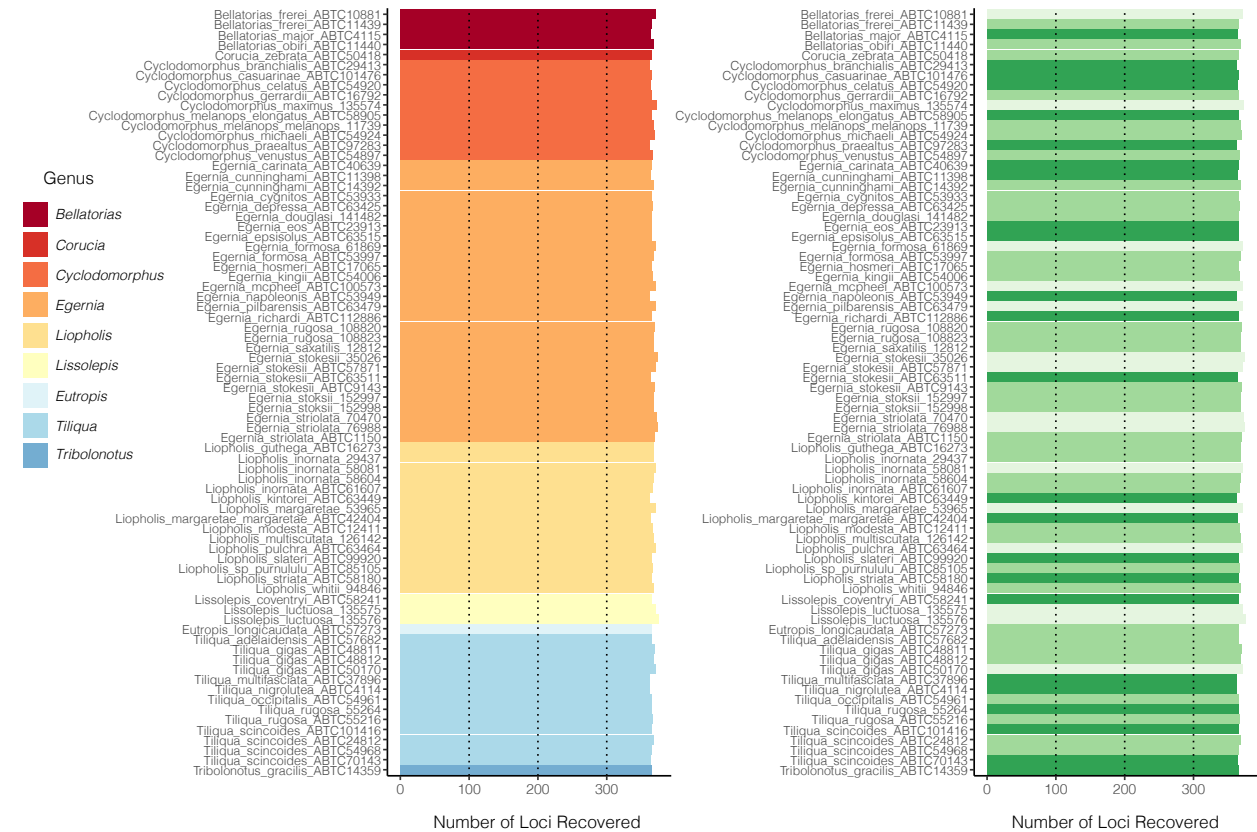


Figure S2: Number of loci recovered per sample for all Tiliquini and outgroup taxa included in the molecular data. Samples are colored by Genus (left) and coverage (right).

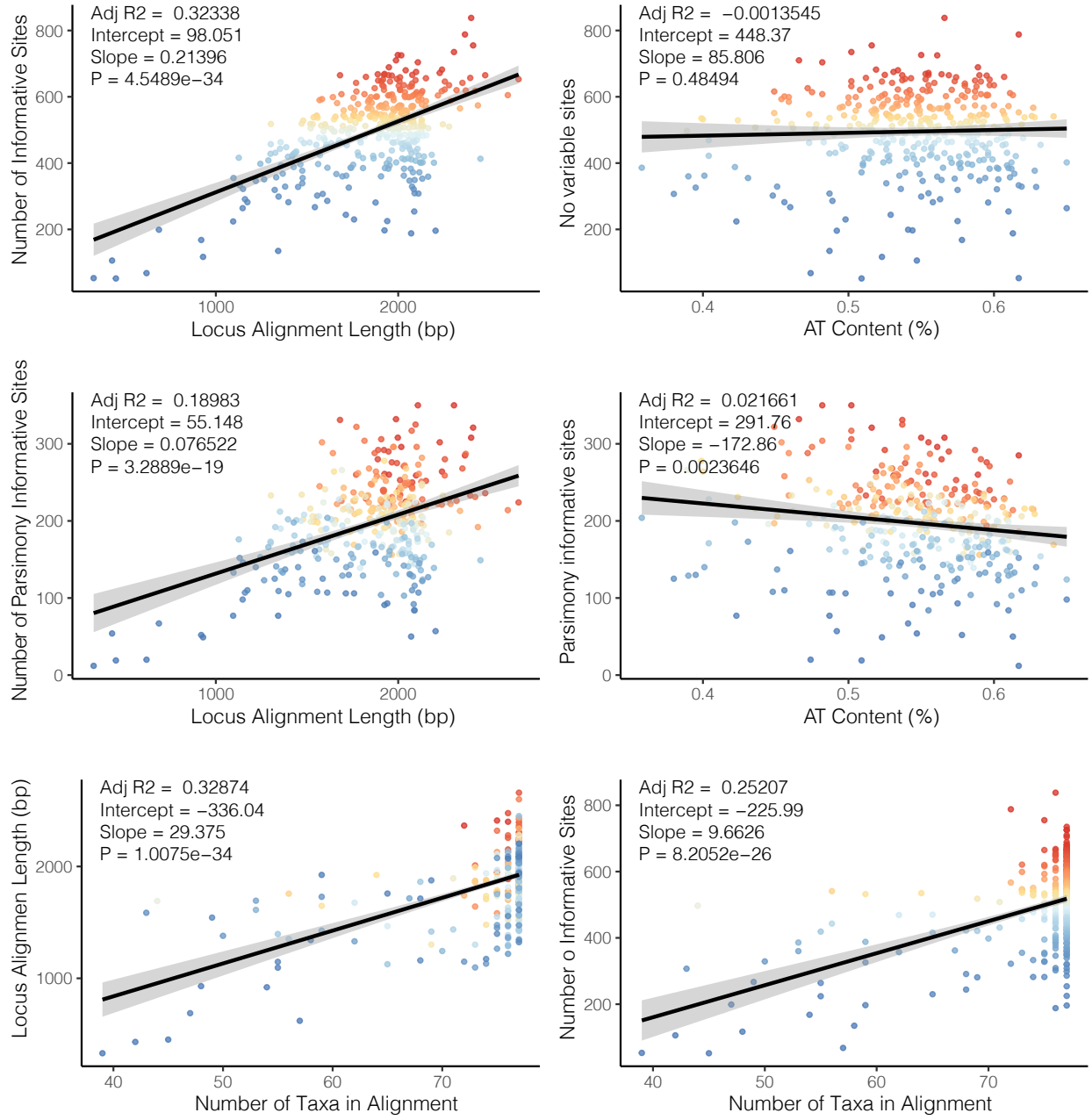


Figure S3: Plots of individual locus completeness and informativeness. Points are colored according to number of informative (variable) sites (blue—few, red—many). Top row shows the number of variable sites in each alignment as a function of alignment length and AT content. The middle row shows the number of parsimony informative sites as a function of alignment length and AT content. The bottom row shows alignment length and number of variable sites as a function of completeness.

Morphological Measurements

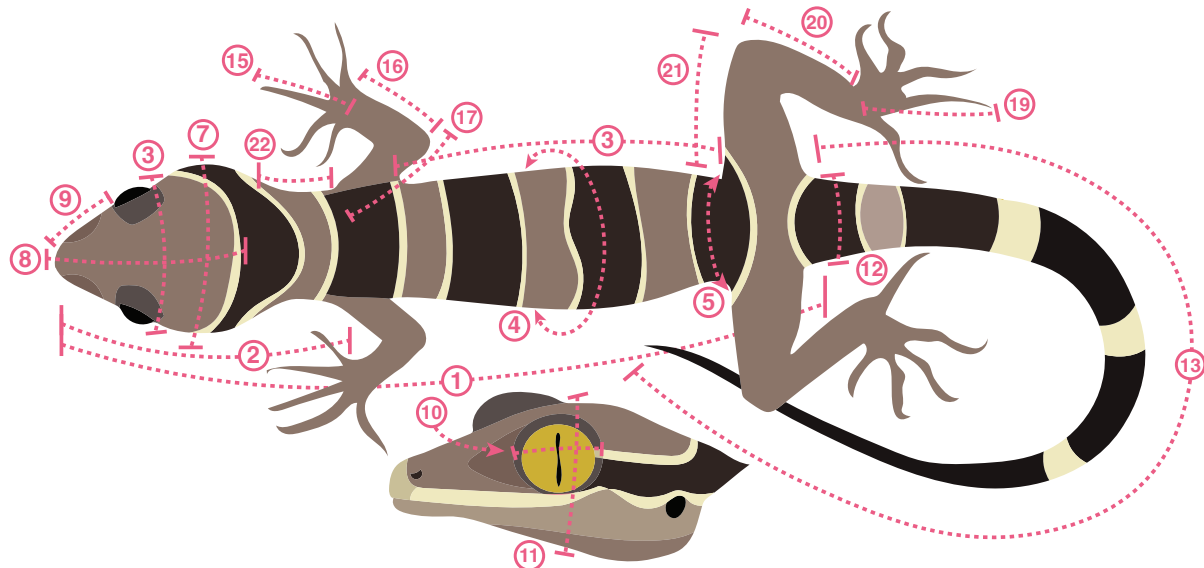


Figure S4: The 21 linear measurements collected.

Initial morphological measurements used for data investigation:

No.	Measurement	Abbreviation	Method
1	Snout-vent length	SVL	From the tip of the snout to the vent.
2	Snout-axilla length	SAL	From the tip of the snout to the midpoint of the crease between the fore-limb and the body on the ventral surface.
3	Inter-limb length	ILL	Midpoint of the crease on the ventral surface where the fore-limb connects to the body, to the midpoint of the crease on the ventral surface where the hind-limb connects to the body.
4	Body width	BW	From one lateral side of the body to the other, where possible at the midpoint of the ILL.
5	Pelvic width	PW	From the midpoint of the crease on the ventral surface where the left hind limb connects to the body, to the midpoint of the crease on the ventral surface where the right hind limb connects to the body.
6	Pelvic height	PH	From the top of the dorsal surface where the PW was measured, to the bottom of the ventral surface where the PW was measured.
7	Head width	HW	Widest part of the head from one

No.	Measurement	Abbreviation	Method
8	Head length	HL	dorsal-lateral edge to the other edge. From the nose tip, to the anterior of the ear.
9	Snout length	SN	From the nasal opening to the anterior of the eye.
10	Eye diameter	ED	From one side of the eye to the other.
11	Head depth	HD	From the top of the tallest part of the head on the dorsal surface, to the bottom of the ventral surface under the jaw.
12	Tail width	TW	Measured at the vent, from one dorsal-lateral edge to the other edge.
13	Tail length	TL	Measured from the vent to the tip of the tail.
14	Fore-limb length	FLL	Measured fully extended from the midpoint of the crease on the ventral surface where the front limb connects to the body, to the end of longest toe (claw included).
15	Front foot	FFOOT	From the base of the foot to the end of the longest toe (claw included).
16	Lower front limb	LFL	Measured from the base of the lower fore limb to the juncture where the limb meets the front foot.
17	Upper front limb	UFL	Measured from the crease on the ventral surface where the fore limb connects to the body, to the end of the lower front limb.
18	Hind-limb length	HLL	From the midpoint of the crease on the ventral surface where the hind limb connects to the body, to the end of longest toe (claw included)
19	Hind foot	HFOOT	From the base of the hind foot to the end of the longest toe (claw included)
20	Lower hind limb	LHL	Measured from the top of the knee joint to the heel juncture where the limb meets the front foot.
21	Upper hind limb	UHL	Measured from the crease on the ventral surface where the hind limb connects to the body, to the end of the knee.

Final morphological traits used for phenotypic analyses:

No.	Measurement	Shorthand	Method
3	Interlimb length	Interlimb	see above
4	Body width	Body_Width	see above
5	Pelvic width	Pelvic_Width	see above
6	Pelvic height	Pelvic_Height	see above

No.	Measurement	Shorthand	Method
7	Head width	Head_Width	see above
9	Snout length	Snout_Eye	see above
10	Eye diameter	Eye_Diameter	see above
11	Head depth	Head_Depth	see above
12	Tail width	Tail_Width	see above
13	Tail length	Tail_Length	see above
17	Upper front limb	Upper_Arm	see above
16	Lower front limb	Lower_Arm	see above
15	Front foot	Hand	see above
21	Upper hind limb	Upper_Leg	see above
20	Lower hind limb	Lower_Leg	see above
19	Hind foot	Foot	see above
22	Neck length	Neck	Snout_Axilla - Head_Length
23	Posterior skull	Pos_Skull	Head_Length - (Snout_Eye + Eye_Diameter)
24	Pelvic gap	Pelvic_Gap	Snout_Vent - (Interlimb + Snout_Axilla)

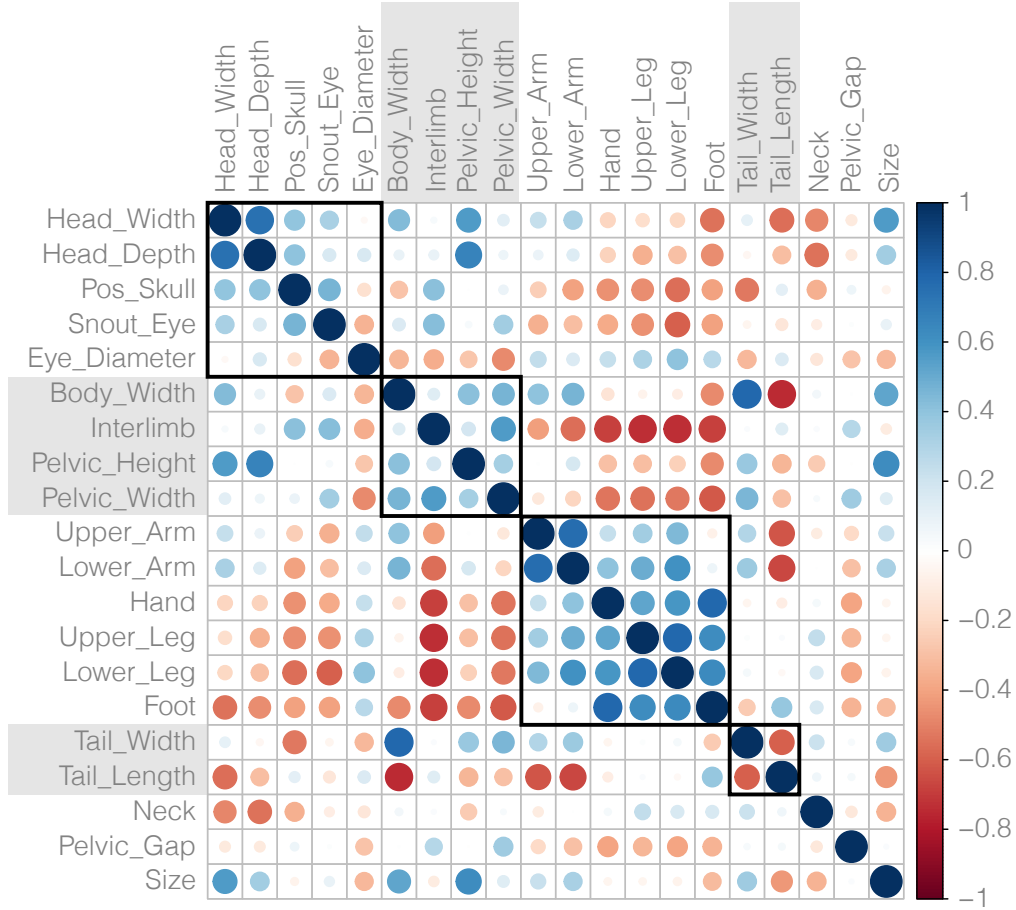


Figure S5: Correlation plot of all morphological traits after removing size via log-shape ratios. Some traits retain strong correlations despite removing the effect of size. Traits are organized according to the morphological module they belong to. Plot generated using *corrplot* [Wei & Simko 2021].

Modelling Trait Evolution and Disparity

- We started by generating mean trait values per species. To remove the effect of size on individual traits (allometry) we then calculated the geometric mean of all traits by species and used this to transform trait measurements into log-shape ratios. This also provided an additional trait *size*. To investigate integrated and modular evolution we estimated correlations among traits and provided this as input for the package *EMMLi* [CITE Goswami & Finarelli]. *EMMLi* also requires *a priori* hypotheses of the assignment of traits to modules. We provided five general hypotheses for model comparison with the most specialized model allowing traits of the head, limbs, body, and tail to evolve as independent modules, and the most restrictive null model lumping all traits into a single module. *EMMLi* also allowed us to compare models in which the correlation coefficient among modules and among traits within modules is either similar or different (see Goswami & Finarelli Fig.2). Once we established the preferred model (head, body, limbs, tail as separate modules with differing inter- and

intramodule correlations) we split our traits into module-specific datasets.

We designed five models of modular evolution for the Tiliquini skink body plan to test integration and modularity via *EMMLi*. (1) a four-module model (*Body_Tail_Limbs_Head*)
690 in which each of the major body regions is isolated as an independent module; (2) a three-
module model (*BodyHead_Tail_Limbs*) where traits of the head and body are combined
into a single module; (3) a two-module model (*BodyHeadTail_Limbs*) in which traits of
the head, body, and tail are combined into a single module; (4) a three-module model
695 (*Body_Head_TailLimbs*) where tail and limb traits make up a single module; and (5) a
two-module model (*BodyHead_TailLimbs*) where body and head traits are one module and
tail and limb traits another.

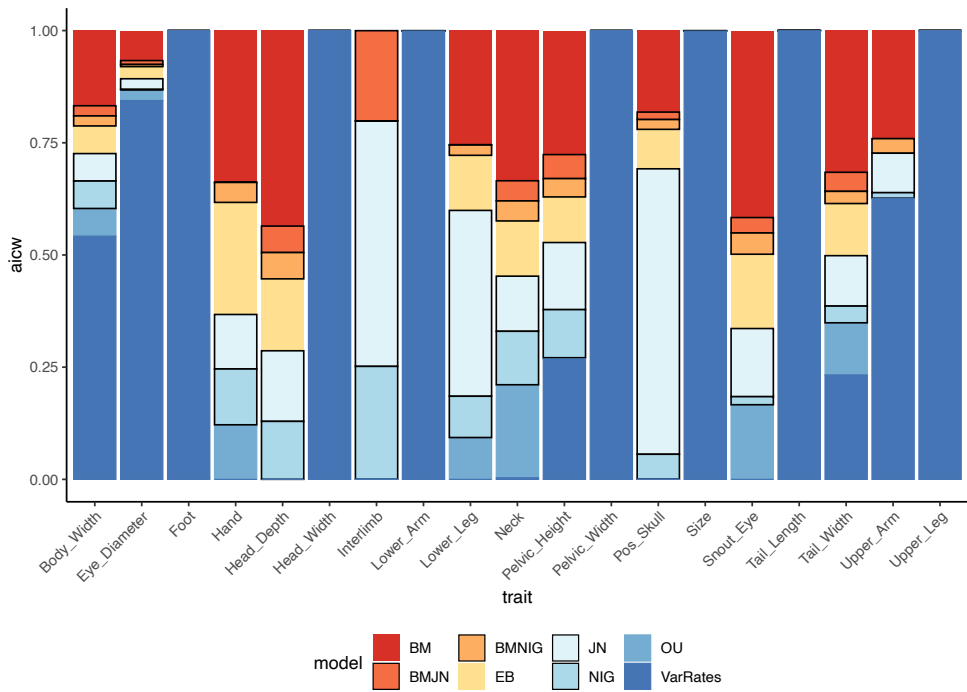
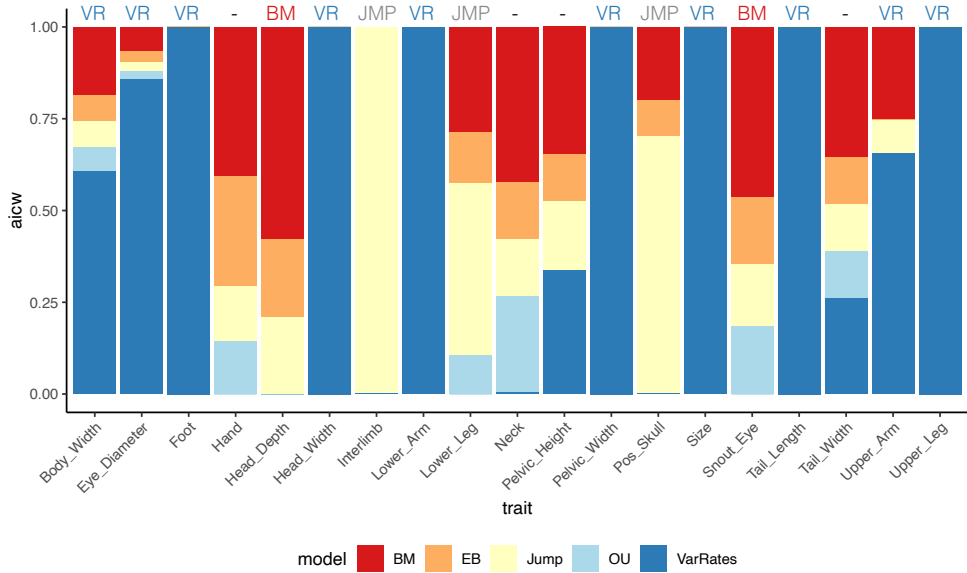


Figure S6: Comparative model fits for each of 19 morphological traits. Upper figure summarizes AICw by model type (BM, EB, ‘Jump’, OU, or VarRates), with the preferred model indicated above the column. Model preference required AICw of the best fitting model to be at least twice that of the next best fitting model. Bottom figure similarly shows model preference but with ‘Jump’ models expanded into their four alternative models (BMJN, BMNIG, JN, NIG) indicated by black outlines.

Concatenation and the Anomaly Zone

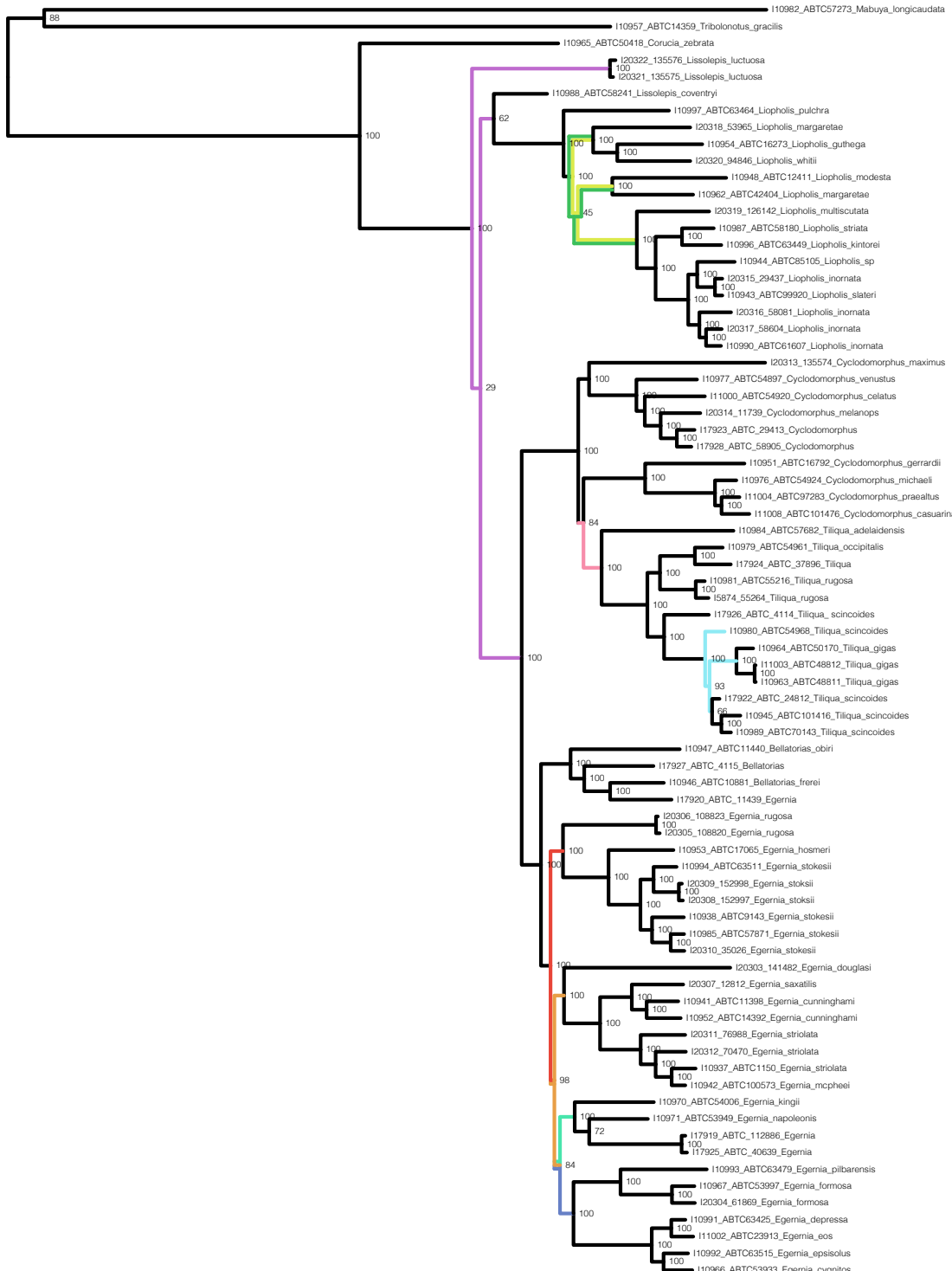


Figure S7: The Tiliquini phylogeny estimated from a concatenated and locus-partitioned alignment is likely misled by branches which fall into the anomaly zone. Colored branches correspond to the anomaly zone cladogram below and indicate edges which differ from the coalescent species tree.

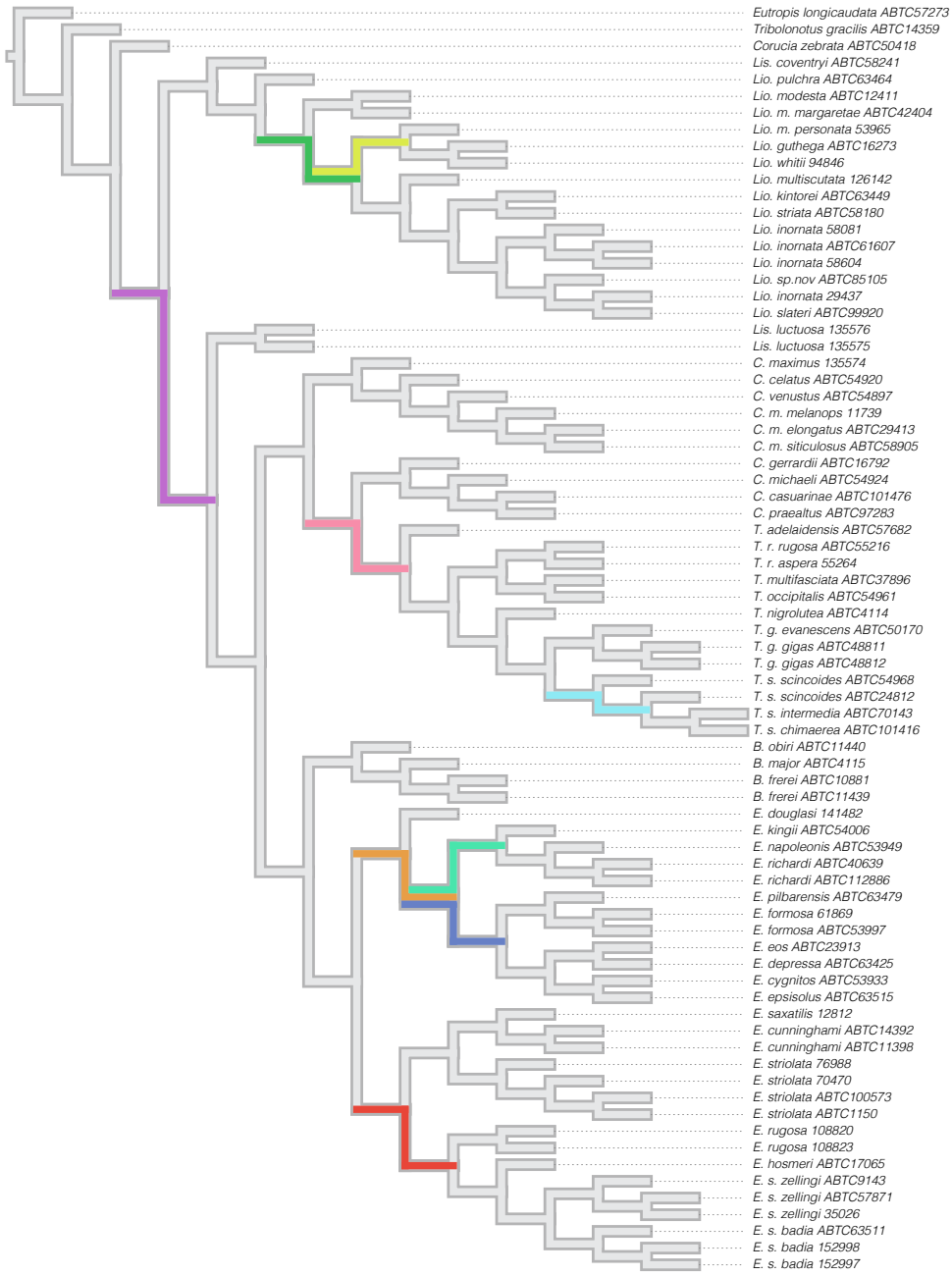


Figure S8: Colored branches indicate edges that fall within the anomaly zone and may provide misleading results under concatenation. We used *Anomaly Finder* [CITE Linkem et al. 2016], using the script from Chafin et al. 2021

Topology Tests

We used a series of topology tests in IQ-TREE to investigate two nodes which bear taxonomic implications. We used the concatenated alignment and simplified phylogenies as the input. In each case the preferred topology is presented first followed by the two alternative resolutions to the bipartition. Significant differences are denoted by (-), and show decisive preference for the coalescent species tree topology in comparison to alternative resolutions, reinforcing molecular phylogenetic evidence for the paraphyly of both *Cyclodomorphus* and *Lissolepis*.

705

Topology test for the paraphyly of *Cyclodomorphus* with regards to *Tiliqua*.
Tree topologies:

- 710
1. (Egernia,(C.maximus,(T.gigas,C.michaeli)); : coalescent/concatenated species trees
 2. (Egernia,(C.michaeli,(T.gigas,C.maximus)); : alternative *Cyclodomorphus* paraphyly
 3. (Egernia,(T.gigas,(C.maximus,C.michaeli)); : *Cyclodomorphus* monophyly

Tree	logL	deltaL	bp-RELL	p-KH	p-SH	p-WKH	p-WSH	c-ELW	p-AU
1.	-1142007.338	0	0.97(+)	0.98(+)	1(+)	0.98(+)	0.993(+)	0.971(+)	0.981(+)
2.	-1142067.499	60.161	0.03(-)	0.02(-)	0.026(-)	0.02(-)	0.039(-)	0.0294(-)	0.021(-)
3.	-1142110.488	103.15	0(-)	0(-)	0(-)	0(-)	0(-)	2.08e-10(-)	1.79e-05(-)

Topology tests for the paraphyly of *Lissolepis*.
Tree topologies:

- 715
1. (Outgroup,((Lis.luctuosa,E.striolata),(Lis.coventryi,Lio._inornata))); : coalescent species tree
 2. (Outgroup,(Lis.luctuosa,(E.striolata,(Lis.coventryi,Lio.inornata)))); : concatenated species tree
 3. (Outgroup,((Lis.coventryi,Lis.luctuosa),(Lio.inornata,E.striolata))); : *Lissolepis* monophyly

Tree	logL	deltaL	bp-RELL	p-KH	p-SH	p-WKH	p-WSH	c-ELW	p-AU
1.	-1326723.218	0	1(+)	1(+)	1(+)	1(+)	1(+)	1(+)	0.995(+)
2.	-1326798.358	75.141	0(-)	0(-)	0.122(+)	0(-)	0(-)	8.47e-07(-)	0.00491(-)
3.	-1327315.329	592.11	0(-)	0(-)	0(-)	0(-)	0(-)	1.9e-174(-)	3.58e-05(-)

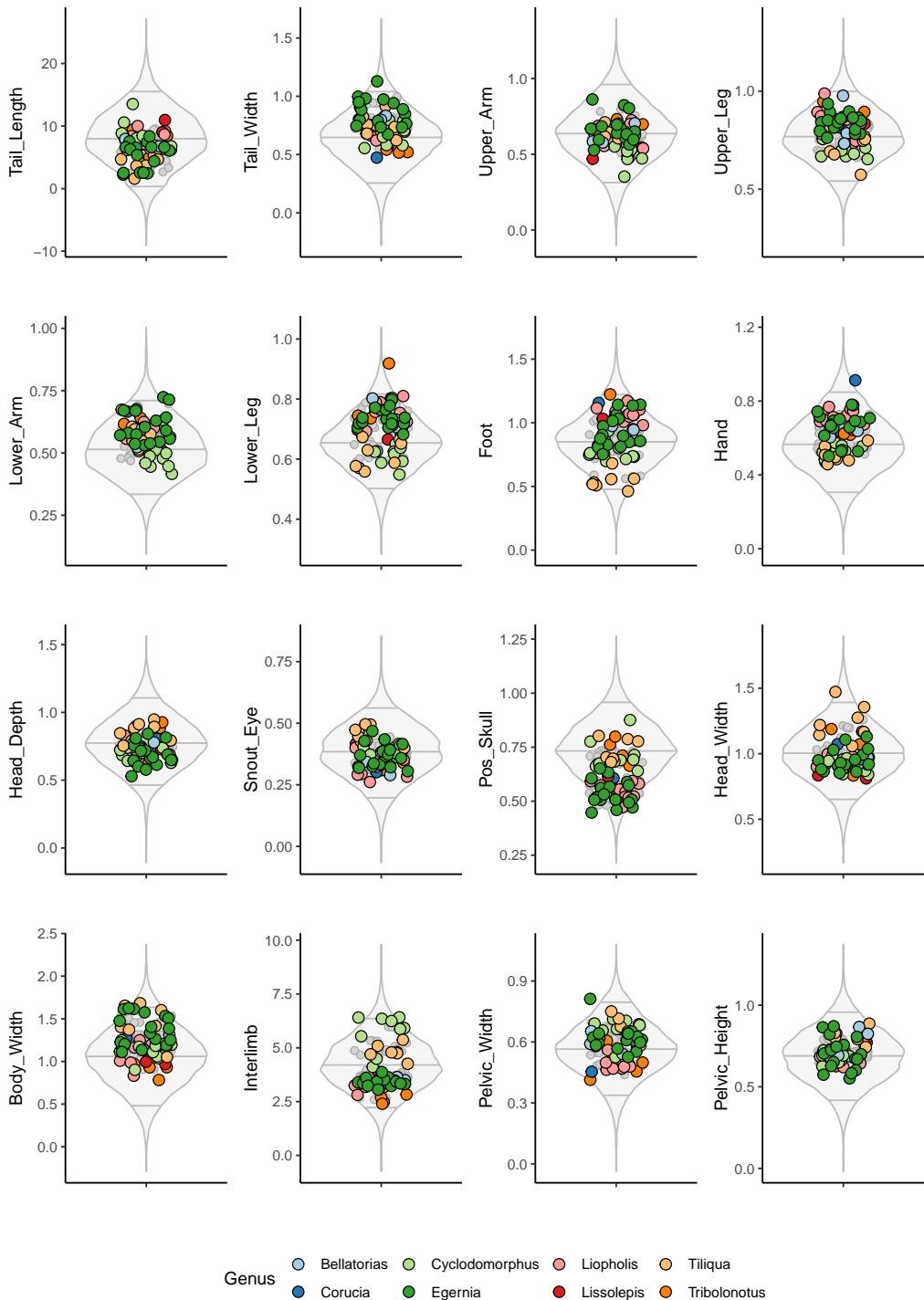


Figure S9: Empirical phenotypes generally conform to expected trait values of data simulated under uncorrelated evolution, showing limited ability of selection to exceed null expectations in Tiliquini skinks. Circles represent empirical trait values per species, colored by genus, with grey representing ancestral states. Transformed traits size corrected by log-shape ratios are plotted against 500 simulated datasets for each trait. Simulated traits are plotted as a grey violin plot summarizing the distribution of trait values, with 5%, 50%, and 95% quantiles plotted as horizontal lines. Simulations were generated with MVMORPH using as input the theta-root and sigma values estimated by MVMORPH assuming a constant-rate Brownian Motion model.

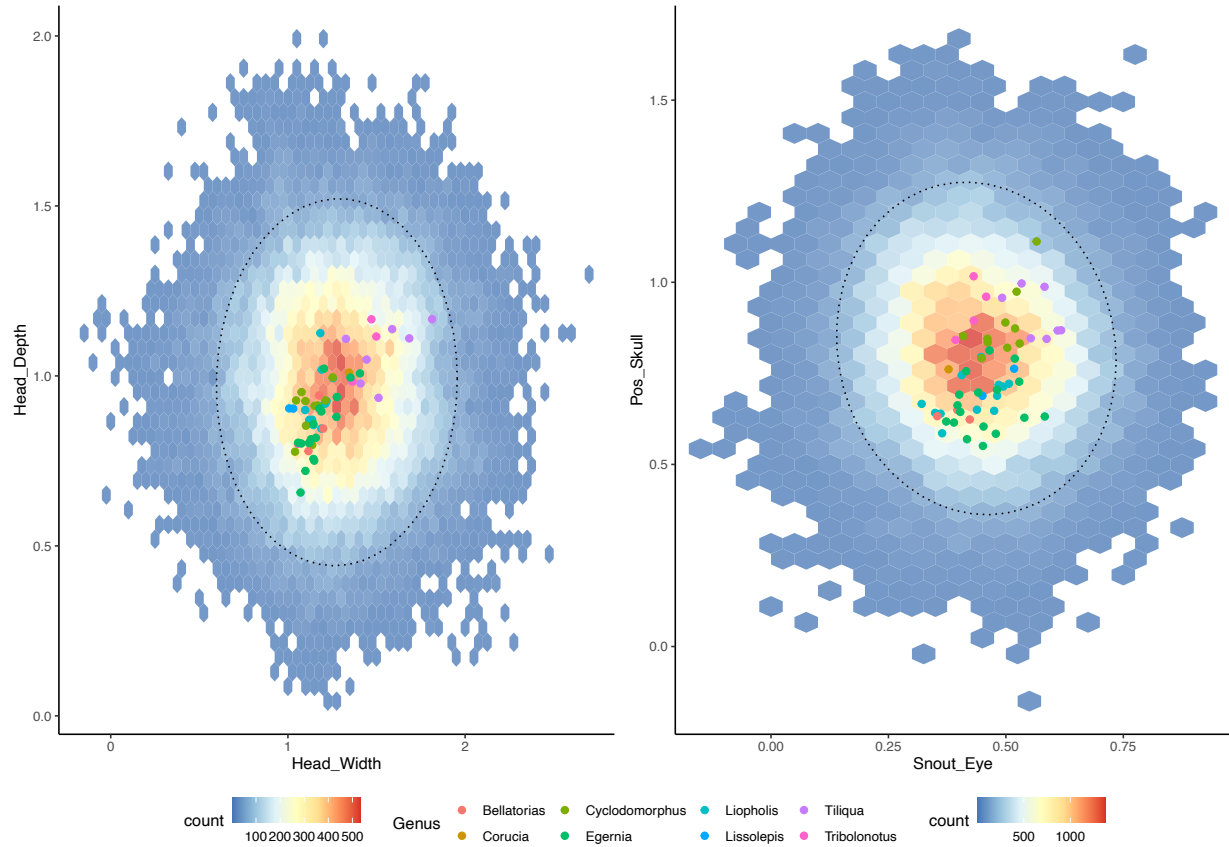


Figure S10: Empirical phenotypes generally conform to expected trait values of data simulated under uncorrelated evolution, showing limited ability of selection to exceed null expectations in Tiliquini skinks. Hexagonal heatplot in background shows the distribution of trait values from 500 datasets simulated under rates from empirical estimates. Warmer colors indicate greater density of simulated points. Circular points indicate empirical trait values and are colored according to the genus the belong to. The dotted ellipse contains 95% of the simulated data (95% confidence interval).

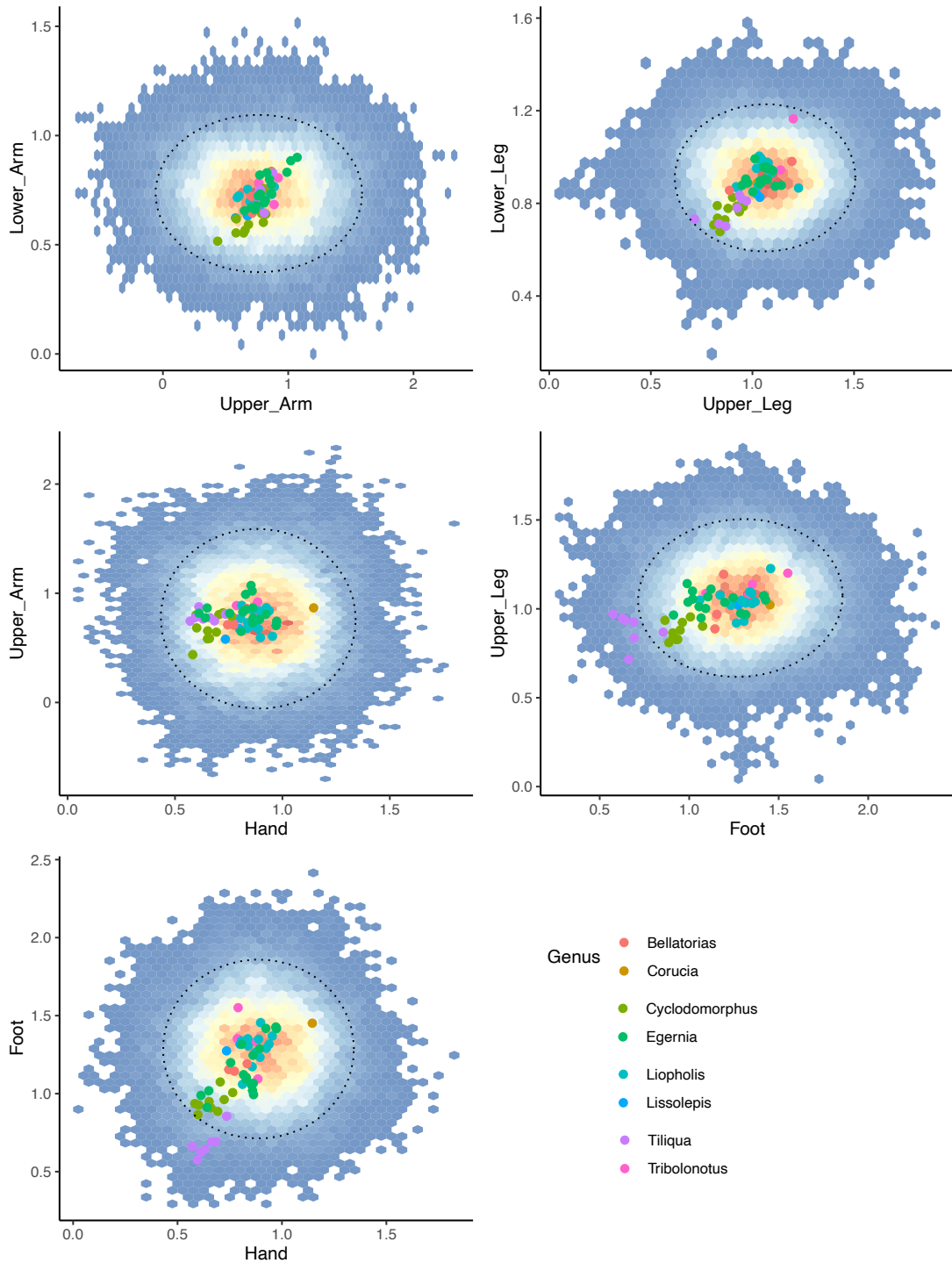


Figure S11: Empirical phenotypes generally conform to expected trait values of data simulated under uncorrelated evolution, showing limited ability of selection to exceed null expectations in *Tiliquini* skinks. Hexagonal heatplot in background shows the distribution of trait values from 500 datasets simulated under rates from empirical estimates. Warmer colors indicate greater density of simulated points. Circular points indicate empirical trait values and are colored according to the genus they belong to. The dotted ellipse contains 95% of the simulated data (95% confidence interval).

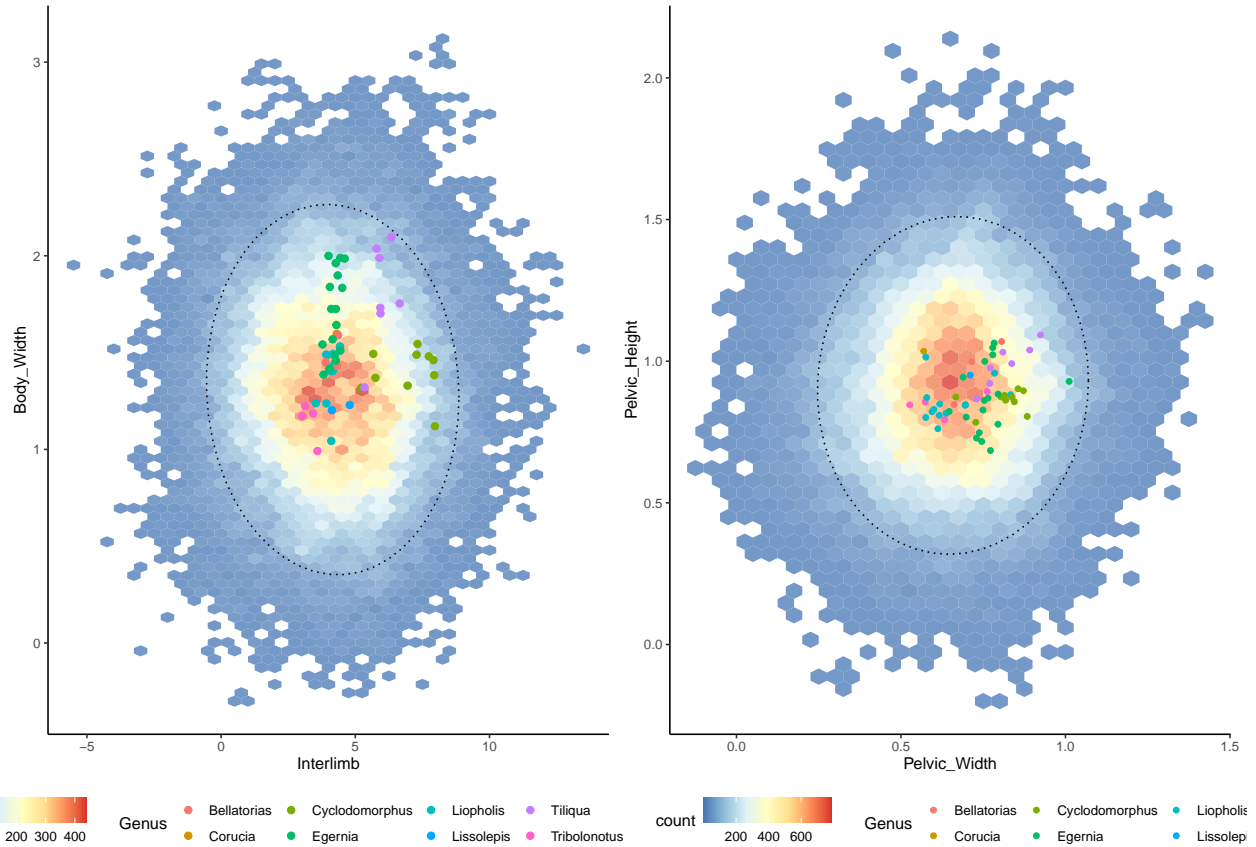


Figure S12: Empirical phenotypes generally conform to expected trait values of data simulated under uncorrelated evolution, showing limited ability of selection to exceed null expectations in *Tiliqua* skinks. Hexagonal heatplot in background shows the distribution of trait values from 500 datasets simulated under rates from empirical estimates. Warmer colors indicate greater density of simulated points. Circular points indicate empirical trait values and are colored according to the genus they belong to. The dotted ellipse contains 95% of the simulated data (95% confidence interval).

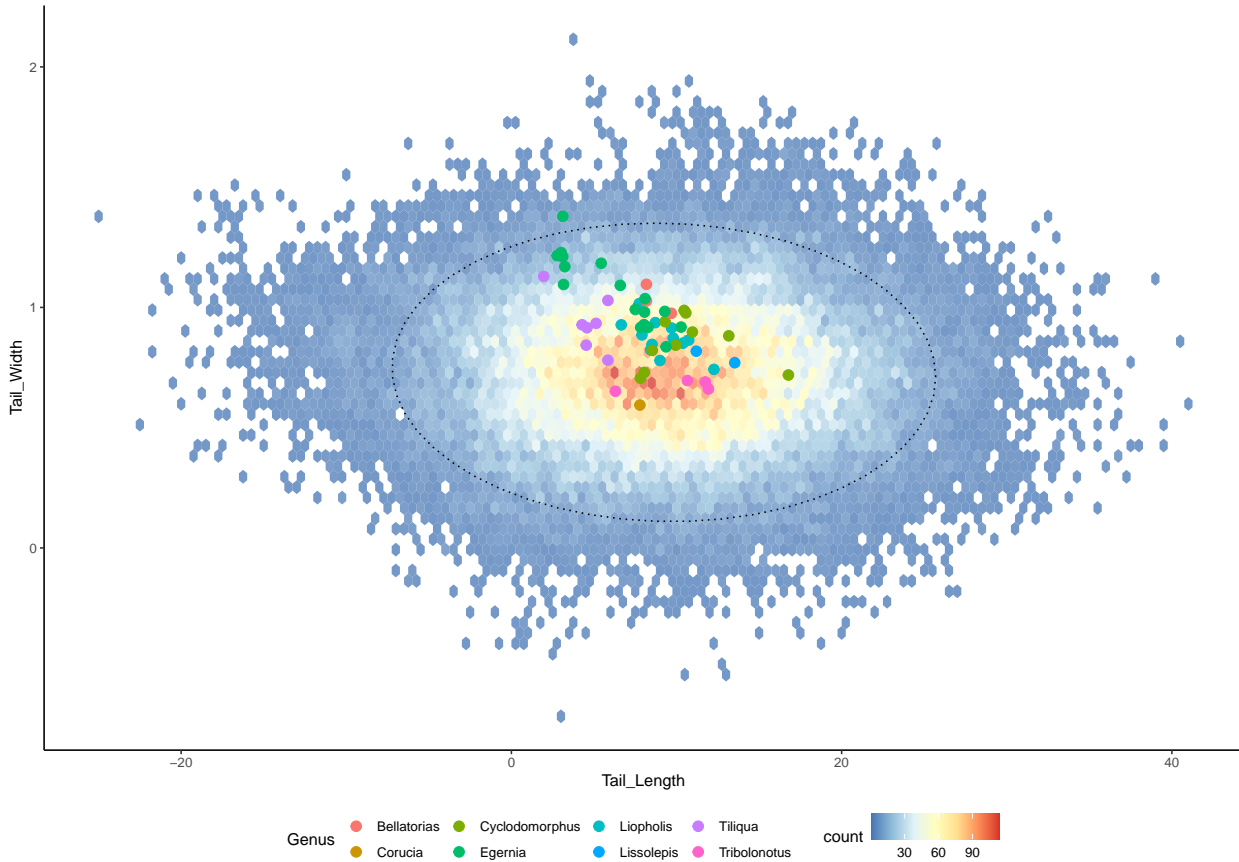


Figure S13: Empirical phenotypes generally conform to expected trait values of data simulated under uncorrelated evolution, showing limited ability of selection to exceed null expectations in Tiliquini skinks. Hexagonal heatplot in background shows the distribution of trait values from 500 datasets simulated under rates from empirical estimates. Warmer colors indicate greater density of simulated points. Circular points indicate empirical trait values and are colored according to the genus they belong to. The dotted ellipse contains 95% of the simulated data (95% confidence interval).

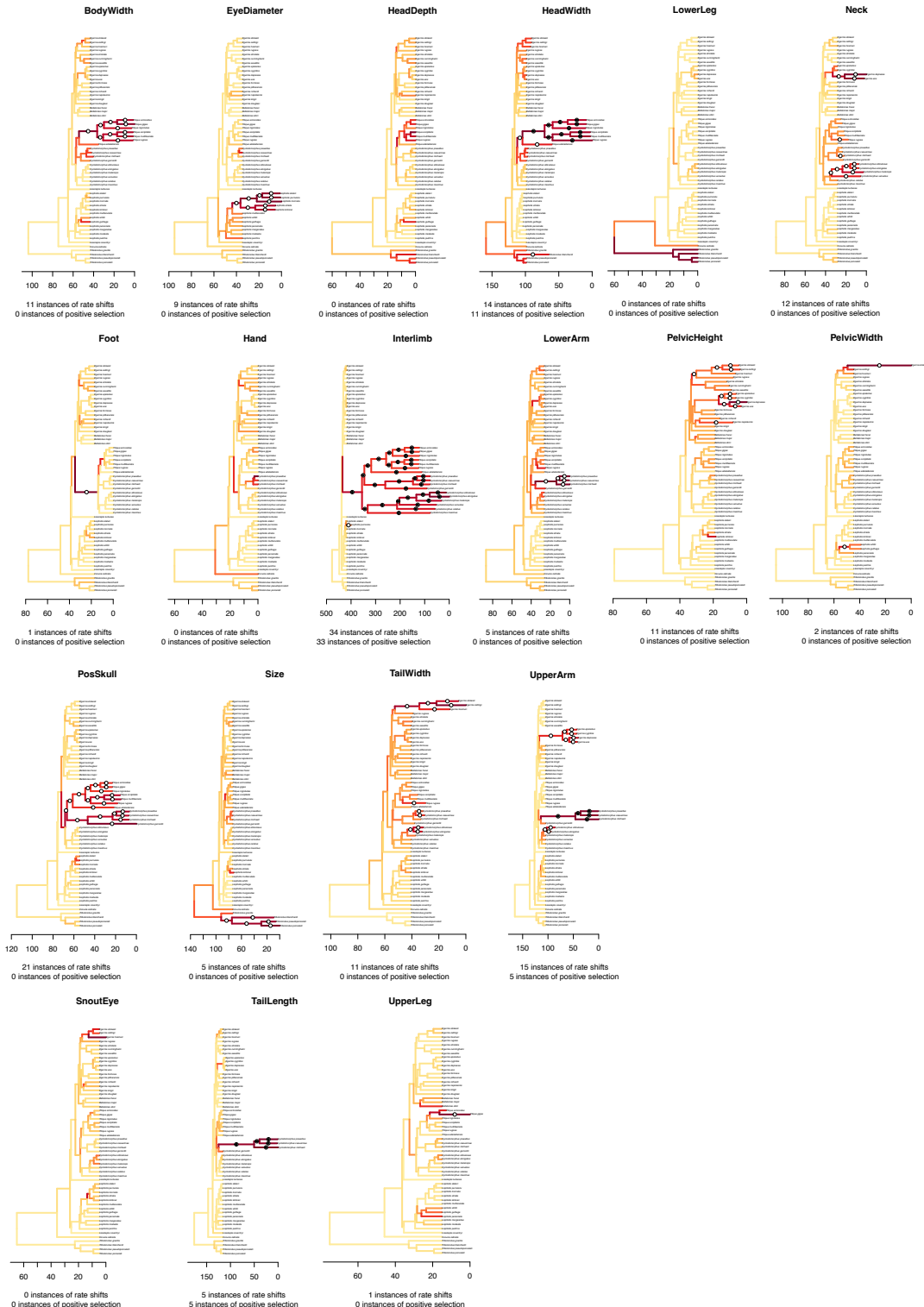


Figure S14: Pulses in rates of phenotypic evolution are common across tiliquine morphological traits. Species trees have been transformed for each trait with branch lengths adjusted relative to the estimated Variable Rates median scalar. Branches are colored according to mean estimated sigma value. Circles indicate significant rate shifts: empty circles represent shifts which appeared in > 70% of the posterior samples and in which the mean estimated scalar > 2; black circles represent shifts which appeared in > 95% of the posterior samples and in which the mean estimated scalar > 2 corresponding to instances of “positive phenotypic selection” per Baker et al. 2017.

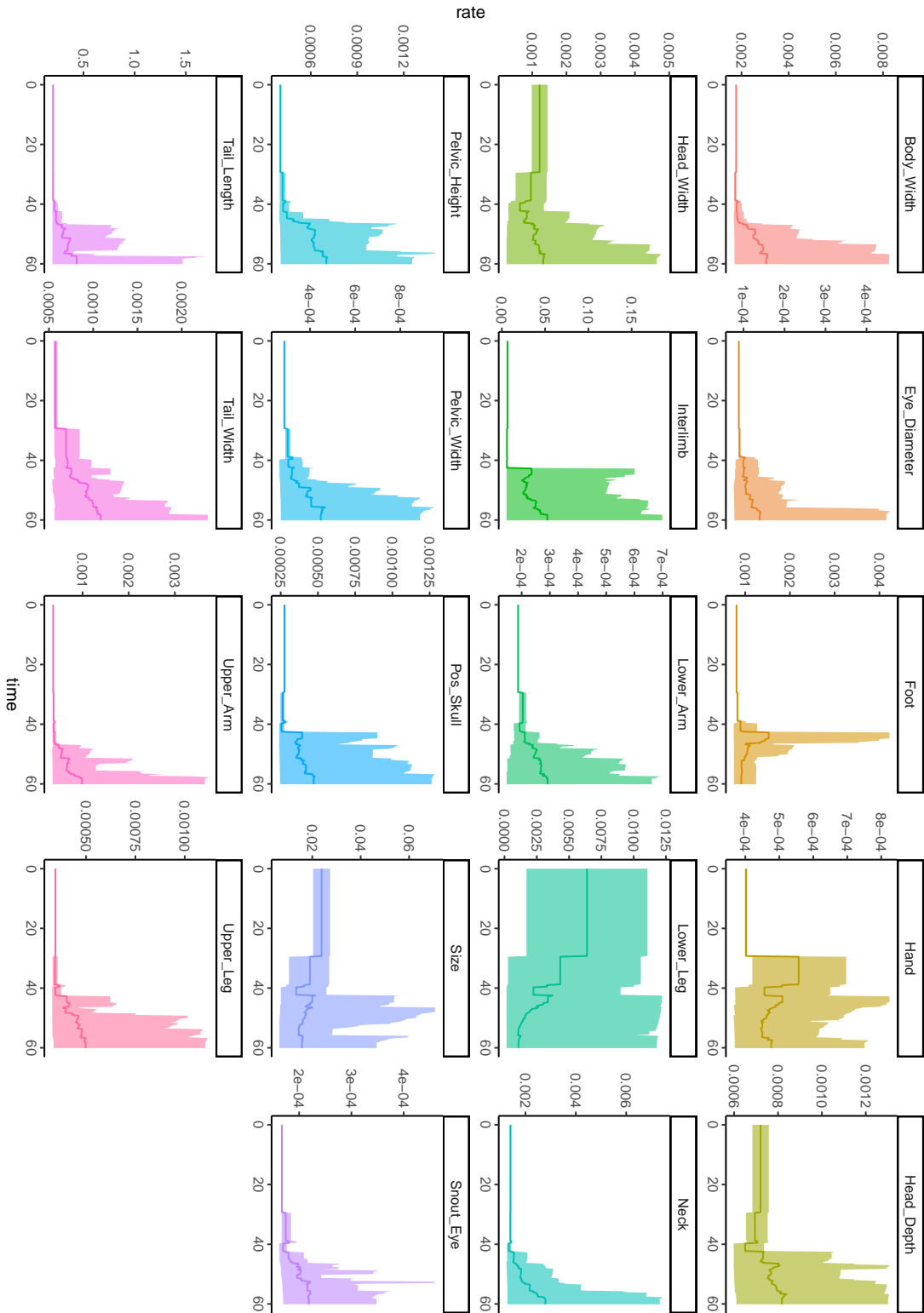


Figure S15: Mean evolutionary rates through time for all morphological traits with envelopes containing 95% quantiles.

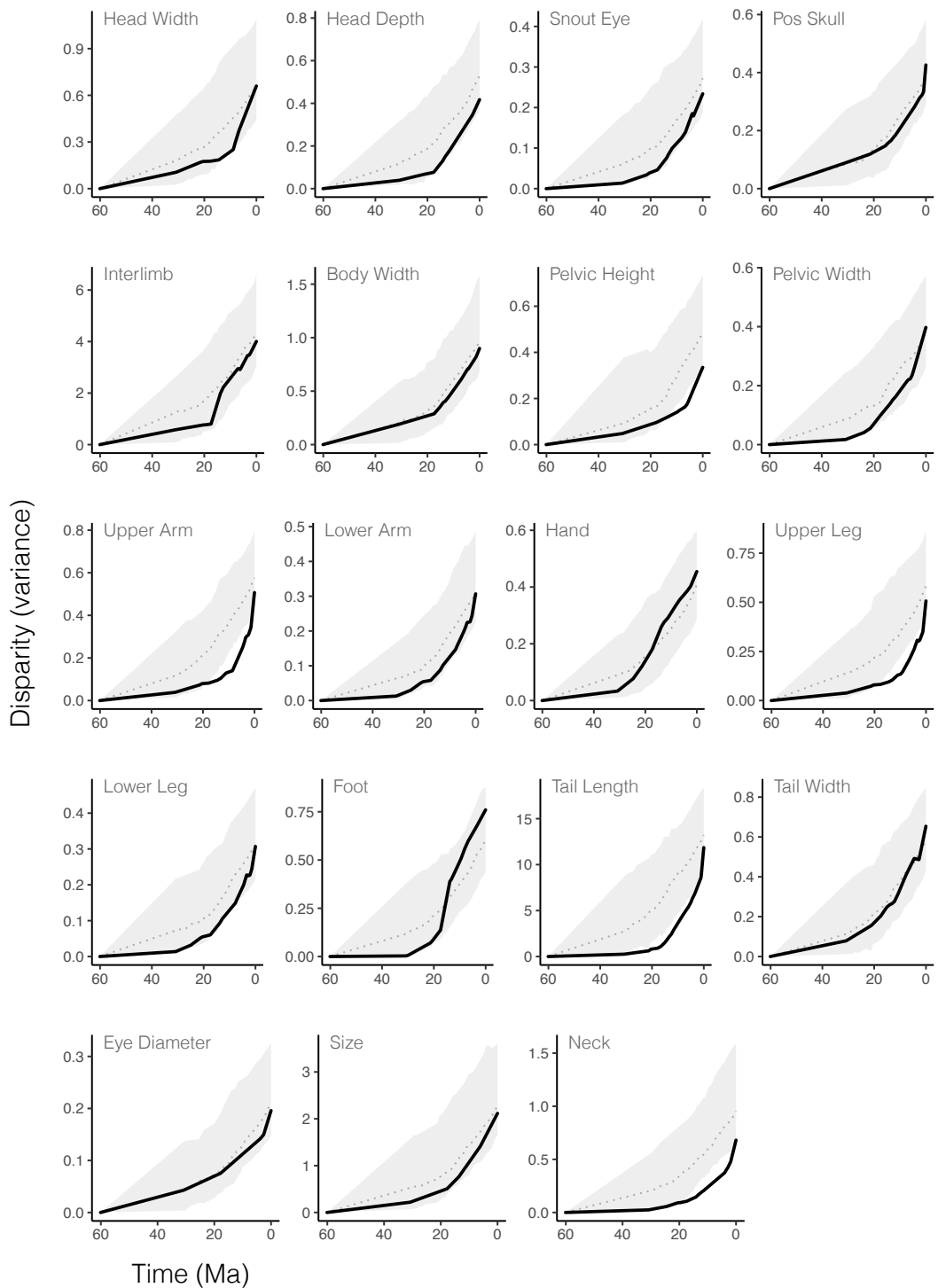


Figure S16: Disparity (variance) through time for morphological traits is often lower than expected under BM for long periods of time early in the evolution of this group. Empirical trends are shown in black with 95% quantiles of disparity for simulated datasets in grey.

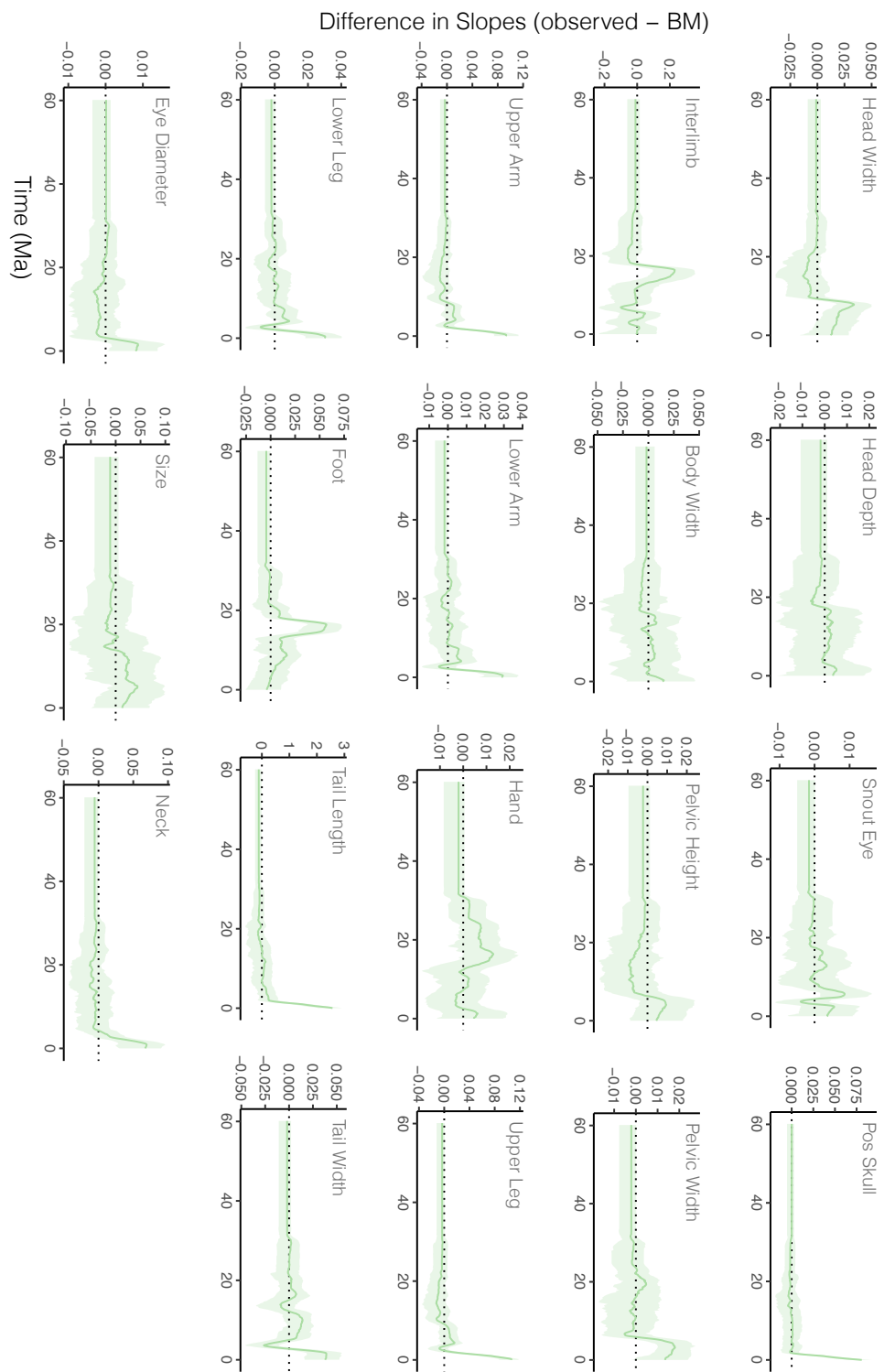


Figure S17: Individual traits show varied temporal patterns of morphological expansion and niche packing. Solid green line shows the mean trend and green envelope shows the 95% quantiles.

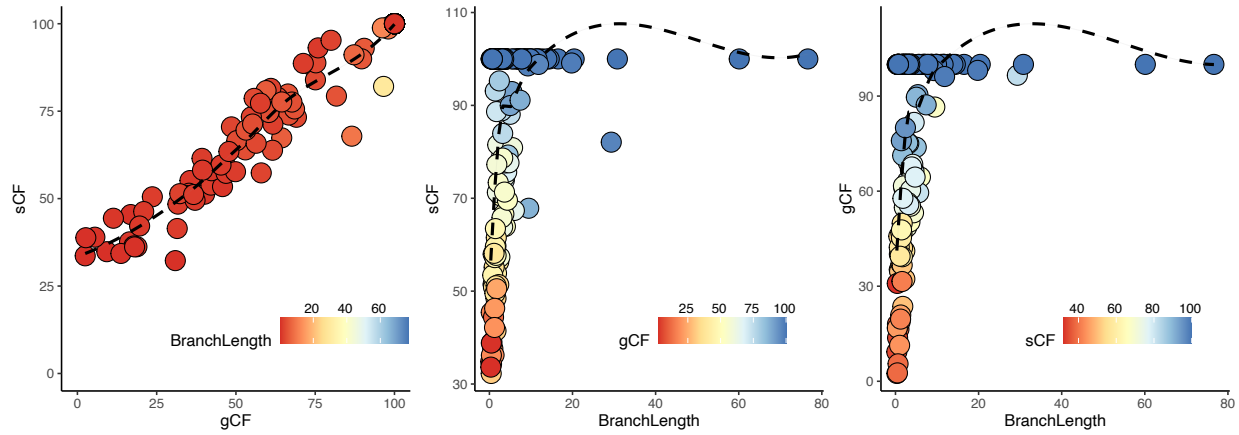


Figure S18: Concordance factors show a positive relationship with increasing branch length. Both site- and gene concordance factors increase support with increasing branch lengths (time), but show saturation ($sCF=100$, $gCF=100$) on branches ≥ 10 million years long.

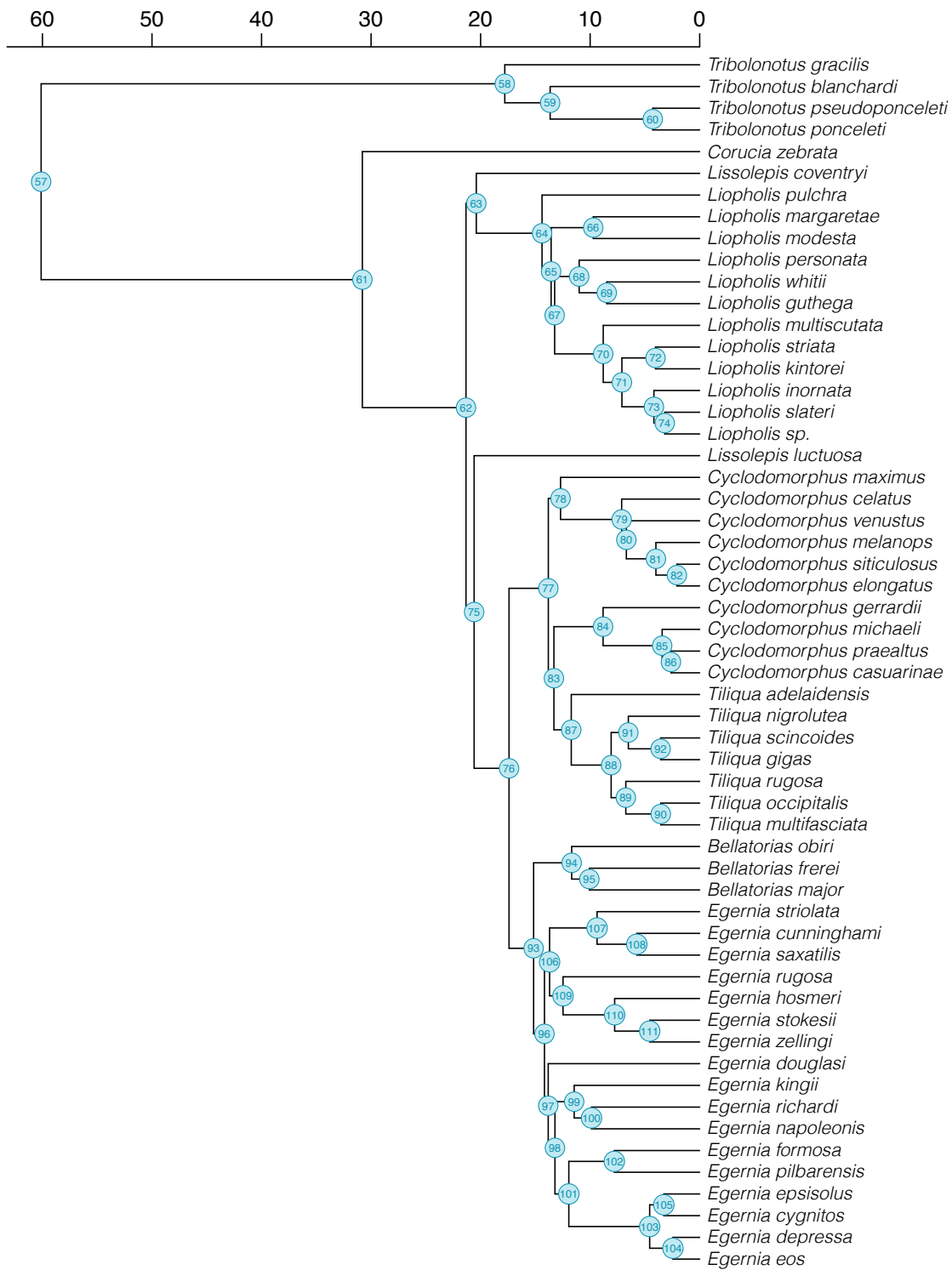


Figure S19: Node numbers of ASTRAL species tree.

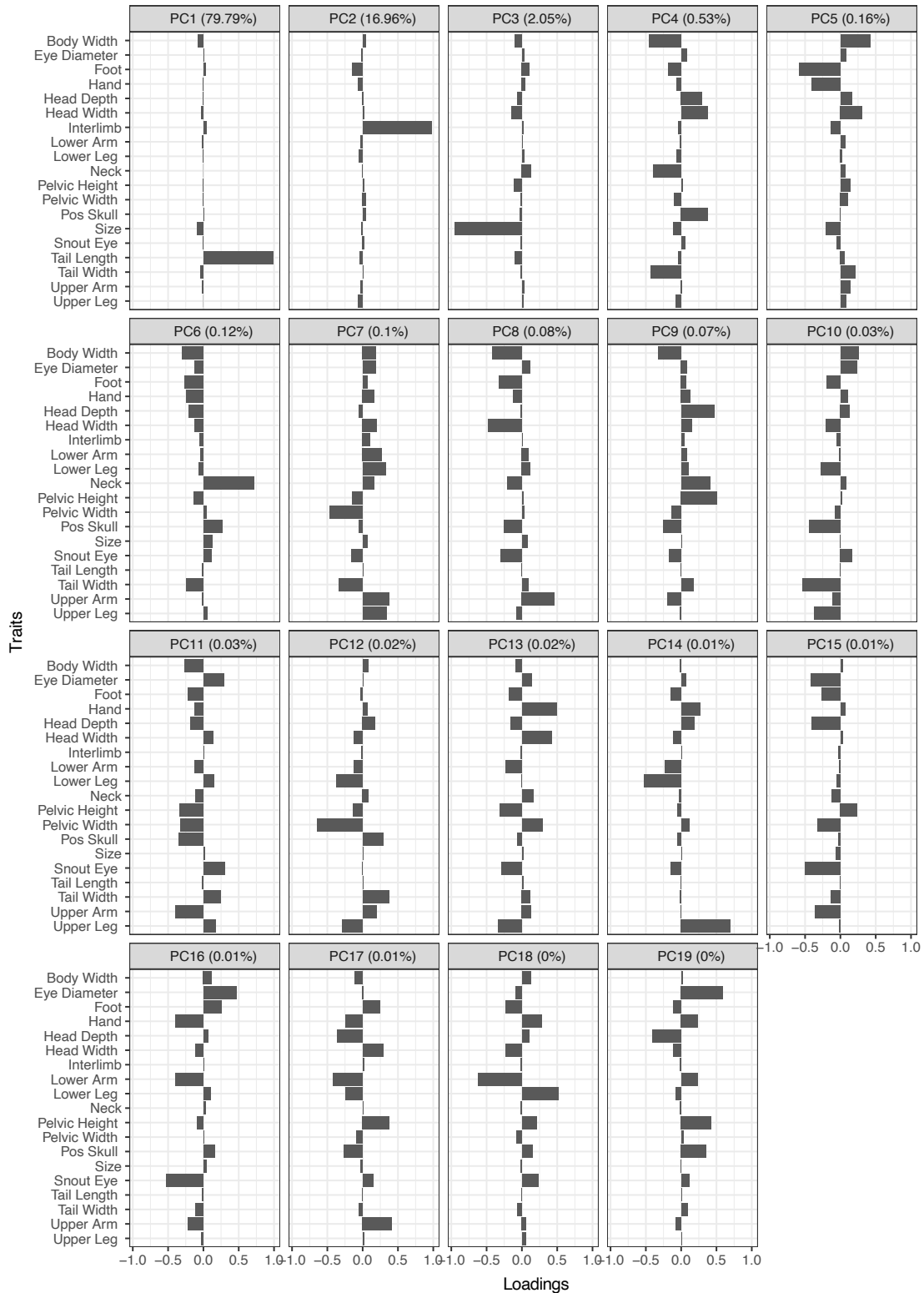


Figure S20: PCA loadings for 19 focal traits across all *Tiliquini* skinks. The first three principal components account for >98% of the variance, and are primarily explained by tail length, interlimb length, and size.

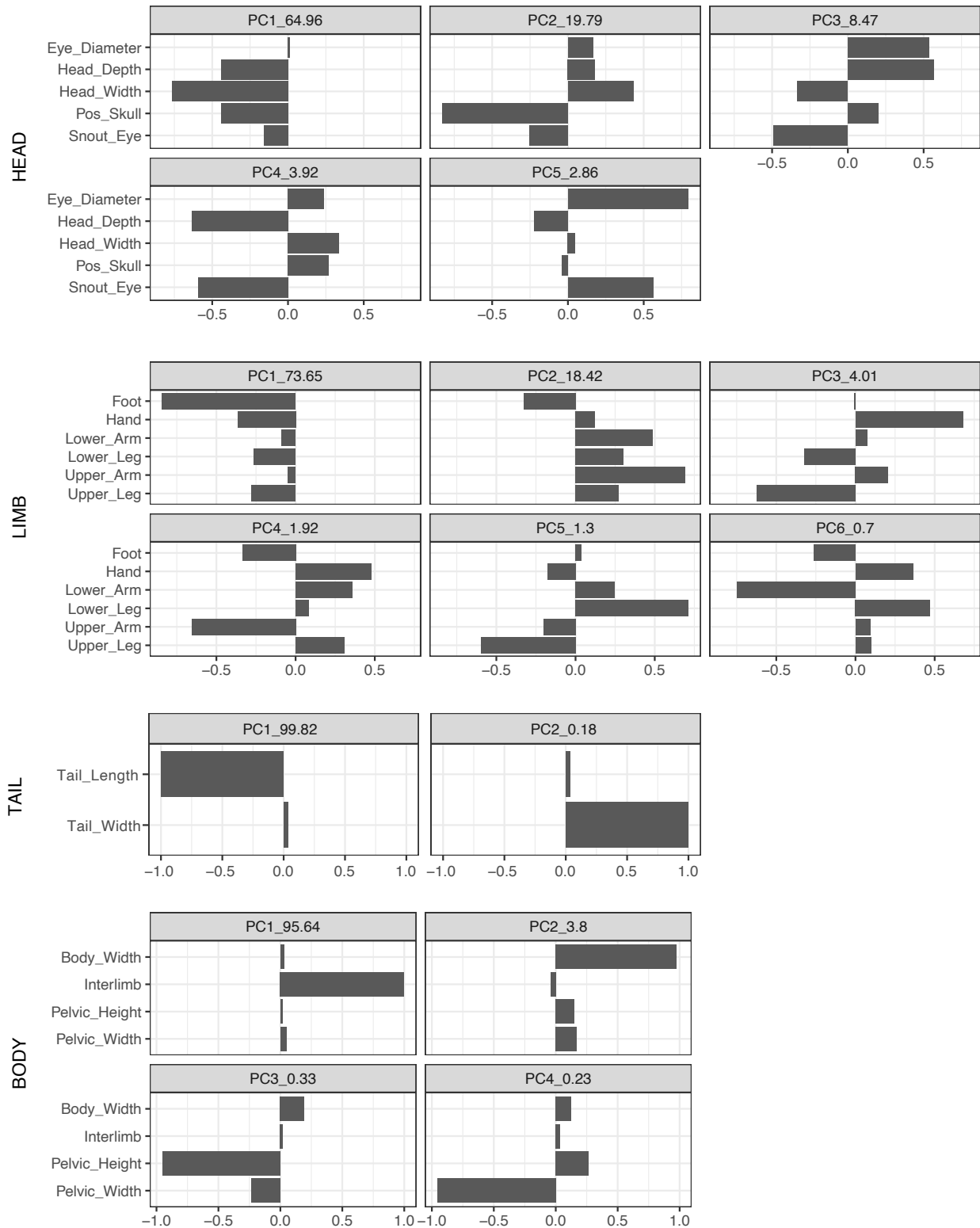


Figure S21: PCA loadings for 19 focal traits analyzed by module across all Tiliquini skinks.

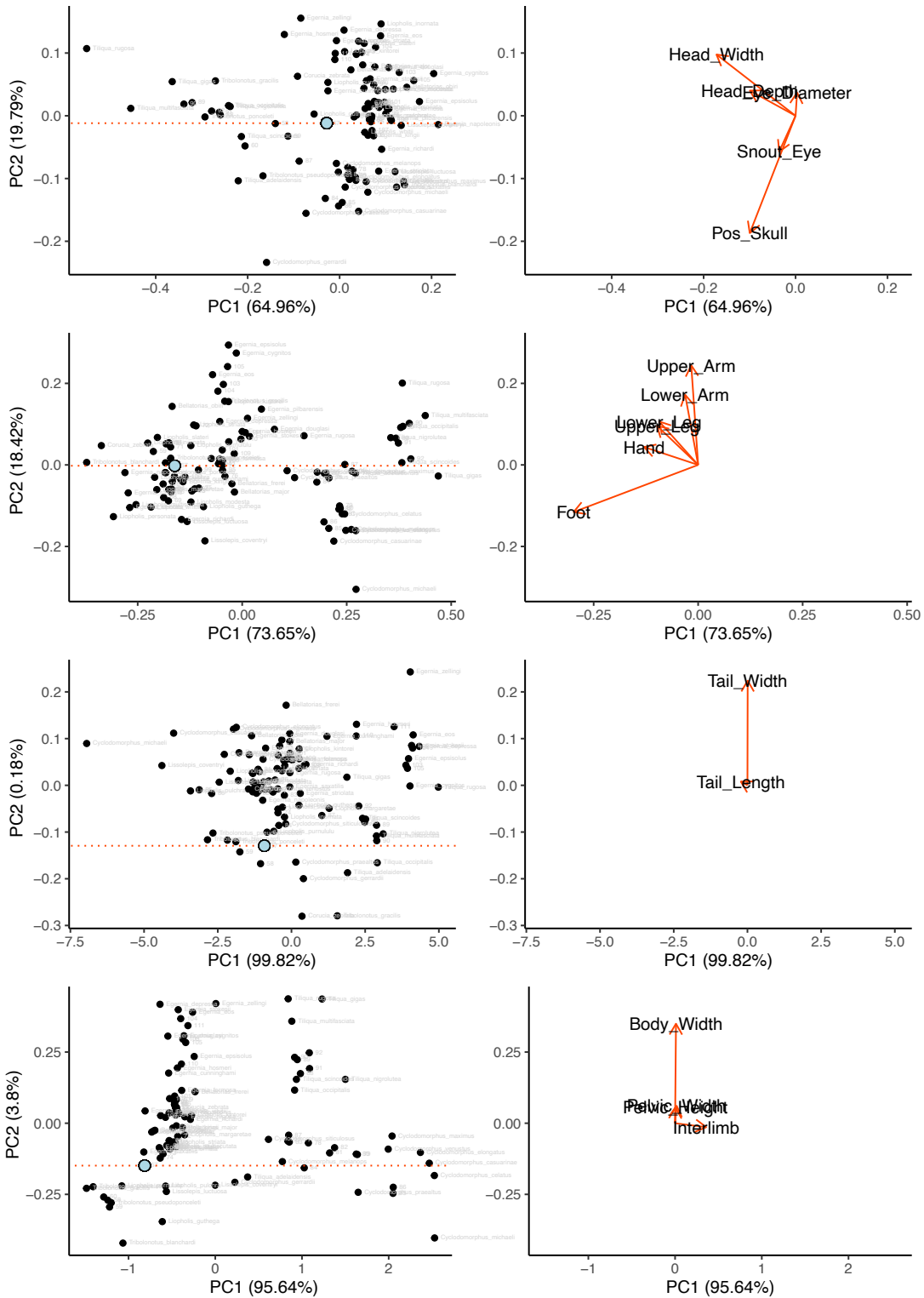


Figure S22: Biplots of the first two PC axes from analyses of modules.

References